Article

Wireless broadband acousto-mechanical sensing system for continuous physiological monitoring

Check for updates

Jae-Young Yoo[1,15], Seyong Oh[2,15], Wissam Shalish[3,15], Woo-Youl Maeng[1,15], Emily Cerier[4], Emily Jeanne[3], Myung-Kun Chung[5], Shasha Lv[3], Yunyun Wu[1], Seonggwang Yoo[1], Andreas Tzavelis[1], Jacob Trueb[1], Minsu Park[6], Hyoyoung Jeong[7], Efe Okunzuwa[4], Slobodanka Smilkova[8], Gyeongwu Kim[9], Junha Kim[10], Gooyoon Chung[10], Yoonseok Park[10], Anthony Banks[1], Shuai Xu[1,11], Guilherme M. Sant'Anna[3], Debra E. Weese-Mayer[12,13,14], Ankit Bharat[4]✉ & John A. Rogers[1]✉

The human body generates various forms of subtle, broadband acousto-mechanical signals that contain information on cardiorespiratory and gastrointestinal health with potential application for continuous physiological monitoring. Existing device options, ranging from digital stethoscopes to inertial measurement units, offer useful capabilities but have disadvantages such as restricted measurement locations that prevent continuous, longitudinal tracking and that constrain their use to controlled environments. Here we present a wireless, broadband acousto-mechanical sensing network that circumvents these limitations and provides information on processes including slow movements within the body, digestive activity, respiratory sounds and cardiac cycles, all with clinical grade accuracy and independent of artifacts from ambient sounds. This system can also perform spatiotemporal mapping of the dynamics of gastrointestinal processes and airflow into and out of the lungs. To demonstrate the capabilities of this system we used it to monitor constrained respiratory airflow and intestinal motility in neonates in the neonatal intensive care unit ($n = 15$), and to assess regional lung function in patients undergoing thoracic surgery ($n = 55$). This broadband acousto-mechanical sensing system holds the potential to help mitigate cardiorespiratory instability and manage disease progression in patients through continuous monitoring of physiological signals, in both the clinical and nonclinical setting.

In 2020, cardiovascular and respiratory diseases were responsible for over 796,000 deaths in the United States, making them the first and third leading causes of death, respectively, in adults, according to the Centers for Disease Control and Prevention[1]. In children and neonates, cardiorespiratory and gastrointestinal problems are major causes of death during the first 5 years of life[2]. The use of continuous monitoring systems can help guide clinical decisions and improve outcomes[3–6]. Current hospital systems continue, however, to rely on

a variety of sensors, wires and cables connected to bedside monitors. Fortunately, advances in bioengineering are leading to the development of broad classes of wireless, skin-interfaced sensors to address these limitations, with easy installation and use in the simultaneous acquisition of multiple classes of signal[3,7–9].

Assessments of cardiac, respiratory and gastrointestinal sounds represent important parts of routine care, because changes in, or absences of, body sounds can represent signs of disease. Digital stethoscopes, including some recently reported in wearable designs, can provide complementary information on cardiac activity, airway obstruction, adventitious lung sounds and intestinal motility[10–17]. These technologies cannot, however, be used effectively for continuous monitoring of those sounds during routine activities due to limitations that include some or all of the following: (1) rigid and bulky engineering designs; (2) inability to support time-synchronized operation across multiple locations of the body; (3) susceptibility to confounding effects of ambient sounds; and (4) sensitivity to noise generated by movements and physical contact. As a result, the clinical use of body sounds for health monitoring occurs typically through episodic measurements, with few examples of applications outside of the hospital.

This paper introduces wireless, skin-interfaced broadband acousto-mechanical sensing (BAMS) systems capable of capturing a wide spectrum of signals, from high-frequency body sounds (up to frequencies of ~1 kHz) to slow body movements (fraction of a hertz, ~0.01 Hz), with capabilities for simultaneous, time-synchronized measurements at several body locations. BAMS systems have several key features that enable practical use in both the hospital and home environment. First, the devices include capabilities for separate, simultaneous recordings of sounds from internal body processes and the external environment because sound is captured using an integrated pair of opposing microphones and interpreted with associated signal-processing algorithms. Second, the small size, lightweight construction, soft mechanical properties and gentle adhesive interfaces allow for measurements from nearly any location of the body and across broad ranges of patients, from premature infants to elderly individuals. Additionally, time-synchronized networks of these sensors, coupled with real-time monitoring technology, allow for quantitative, continuous tracking of essential body sounds ranging from multiple aspects of cardiorespiratory function, gastrointestinal activity, swallowing and respiration and spatially mapped dynamic properties of airflow into and out of the lungs. Here we report the successful deployment of these BAMS systems in monitoring and providing clinical data for premature infants in neonatal intensive care units (15 neonates) and adult patients (55 participants) in the thoracic surgery clinic. The following describes the detailed engineering aspects of these technology platforms, quantifies their various measurement capabilities and, where possible, compares the results to state-of-the-art, clinically approved technologies.

Results

The BAMS network system

Figure 1a illustrates three clinically relevant applications of the BAMS network system where recordings capture sounds and physical motions across a frequency range from 1 kHz to near 0 Hz. Gentle adherence of a single device at the suprasternal notch allows for simultaneous measurement of cardiac and respiratory sounds, providing continuous monitoring of cardiorespiratory activity (Fig. 1a, left). Time-synchronized devices placed on the abdomen enable spatiotemporal monitoring of gastrointestinal sounds for tracking the progress of digestion (Fig. 1a, middle). An advanced implementation involves 13 wirelessly time-synchronized devices placed at targeted sites across the anterior and posterior chest for regional monitoring of pulmonary health, rehabilitation and disease progression (Fig. 1a, right). The applicability of this technology spans across nearly any type of patient and age, from premature babies in neonatal intensive

care units (NICUs) to patients with chronic lung diseases in the outpatient clinic or in the intensive care unit, and to patients following lung resection, as demonstrated in the following sections. The picture in Fig. 1b shows a BAMS device on a neonate model positioned for cardiorespiratory monitoring. A real-time graphical user interface displays quantitative information on body movements and a spectrogram of body sounds at 100-ms intervals, thereby capturing parameters such as body orientations and physical activities, along with sound intensities and frequencies associated with both the body and ambient sounds. Data communication exploits standard Bluetooth low-energy (BLE) protocols.

Figure 1c depicts an exploded-view illustration of a BAMS device that incorporates an inertial measurement unit (IMU; LSM6DSL, STMicroelectronics), a pair of microphones (ICS-40180, TDK)—one body-facing (toward the body) and the other ambient-facing (toward the surroundings)—a BLE system on a chip (SoC; ISP-1807, Insight SIP), a 2-GB flash memory (MT29F2G, Micron) and a wireless-charging antenna, all mounted on a flexible printed circuit board. The BAMS system achieves broadband operation by combining an IMU and a pair of microphones with an analog-to-digital converter with high sampling rate, thereby enabling detection of signals across a wide frequency range, from measurements of body orientation (fraction of a hertz, ~0.01 Hz) to body sounds (~500 Hz). The three-axis acceleration data captured by the IMU relate to body orientation (~0 Hz), body motion (~1 Hz) and physical activity (~20 Hz) without interference from ambient sounds[4,18–20]. The IMU lacks, however, the sensitivity required to measure subtle body sounds such as those associated with detailed features of respiratory and cardiac activity and bowel movements. In contrast, the microphone system exhibits high sensitivity in the frequency range 20 Hz to 20 kHz, making it efficient for capturing even weak body sounds up to frequencies limited by the analog-to-digital converter in the BLE SoC (~20 kHz samples s^{-1}). An advanced capability of the technology reported here lies in the high-fidelity measurements of body sounds achieved through the integration of a pair of opposing microphones. These body- and ambient-facing microphones allow selective measurements of body and ambient sounds, using algorithms described below. The spectral and temporal characteristics of body sounds, without the confounding effects of ambient sounds, provide insights into essential activities associated with respiration, digestion, subaudible vocalizations and cardiac cycles as the basis of diverse, clinically actionable information for patient care (Fig. 1d). Separate measurements of ambient sounds provide essential circumstantial information that can be important in clinical decision making. The IMU and microphone sensors exhibit stable performance with deviations of 0.1 and 0.4%, respectively, within the typical body temperature range of 32–40 °C. This stability enables reliable and consistent use in various clinical cases (Supplementary Fig. 1). Real-time data analytics on the time-series data related to body sounds enable detection of risk events ranging from tachycardia and bradycardia to severe wheezing/coughing, apneic events and digestive abnormalities. A light-emitting diode encapsulated within the device structure can be activated based on threshold settings to serve as an alarm to caregivers, in addition to providing warnings and phone calls that can be initiated through the user interface (Extended Data Fig. 1).

Figure 1e shows the results of cardiorespiratory monitoring using a US Food and Drug Administration (FDA)-approved electrocardiographic (ECG) device and a monitoring system for exhaled CO_2, together with the output of a single BAMS device located at the suprasternal notch of a 19-month-old infant. High-pass ($f_{cut\text{-}high}$ = 150 Hz) and low-pass ($f_{cut\text{-}low}$ = 150 Hz) filtering applied to the microphone data isolate the sounds of respiratory and cardiac activity, respectively. Passing the acceleration data through a bandpass filter ($f_{bandpass}$ = 0.1–1 Hz) yields signals related to movements of the chest. The results exhibit strong correlations between chest movements, respiratory sound
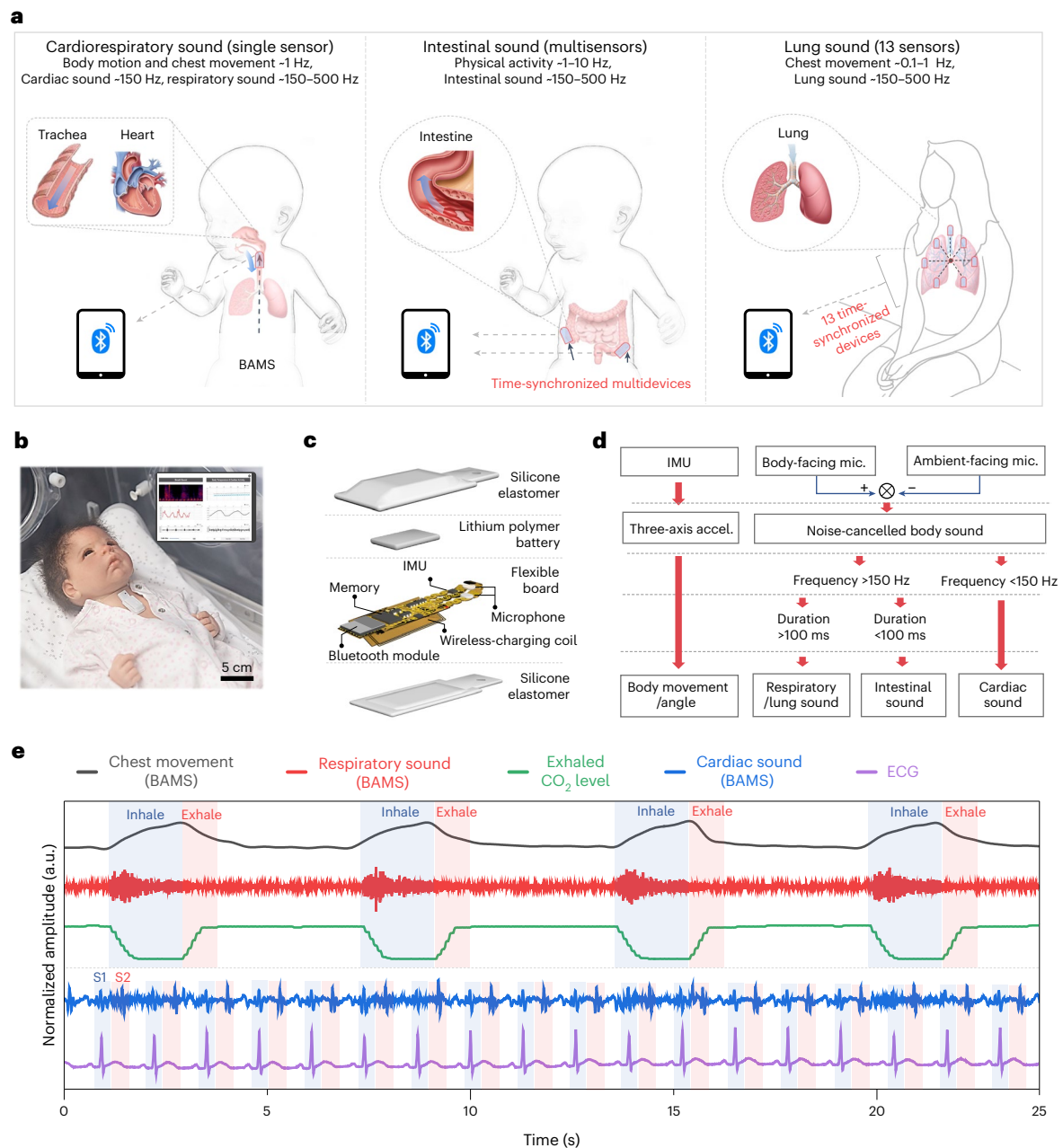
Fig. 1 | Wireless networks of skin-interfaced miniaturized sensors of body sounds and motion for continuous physiological monitoring and diagnostics. a, Schematic illustration of our system for tracking cardiorespiratory activity, gastrointestinal sounds and multilocation respiratory sounds. **b**, Photograph of a BAMS device on a neonatal model. Inset, the associated real-time graphical user interface. **c**, Schematic exploded-view illustration of a BAMS device. **d**, Block diagram of the physiological monitoring scheme that combines an IMU with both body- and ambient-facing microphones (mic.). accel., acceleration. **e**, Comparison of clinical results obtained with a BAMS device (chest wall movements, gray trace; respiratory sounds, red trace; cardiac sounds, blue trace) with standard clinical systems for ECG monitoring (purple trace) and exhaled CO_2 tracing (green trace), from a 19-month-old patient in the pediatric intensive care unit. The blue area in both cardiac sounds and ECG signal represents the respective positions of the S1 peak in the former and the R peak in the latter, while the red area represents the positions of peaks S2 and T, respectively. a.u., arbitrary units.

intensities and exhaled CO_2 levels, signifying respirations. Also, the S1 and S2 features associated with cardiac sounds align with the R and T peaks of the ECG data, as expected. Supplementary Table 1 presents a comparison of data collected using the BAMS device with both a recently reported wearable stethoscope and a commercial stethoscope (3M Littmann CORE, Eko)[14,21–25]. The BAMS system is much smaller (240 times smaller in volume) and lighter (21 times lower in weight) than this commercial stethoscope, thereby allowing for continuous, hands-free monitoring. The soft and flexible mechanical properties

of the BAMS system, the ability to record separate measurements of body and ambient sounds and the capacity for time-synchronized operation across a wireless network of devices represent additional distinguishing features. Additionally, the low power consumption of the BAMS system (in standby mode, 0.036 mA at 3.7 V; in active mode, 2.8 mA at 3.7 V) allows for extended periods of continuous monitoring lasting up to 29 h. Furthermore, the system features a wireless scheme that enables charging of a fully depleted battery to its full state in approximately 4 h (Supplementary Fig. 2).
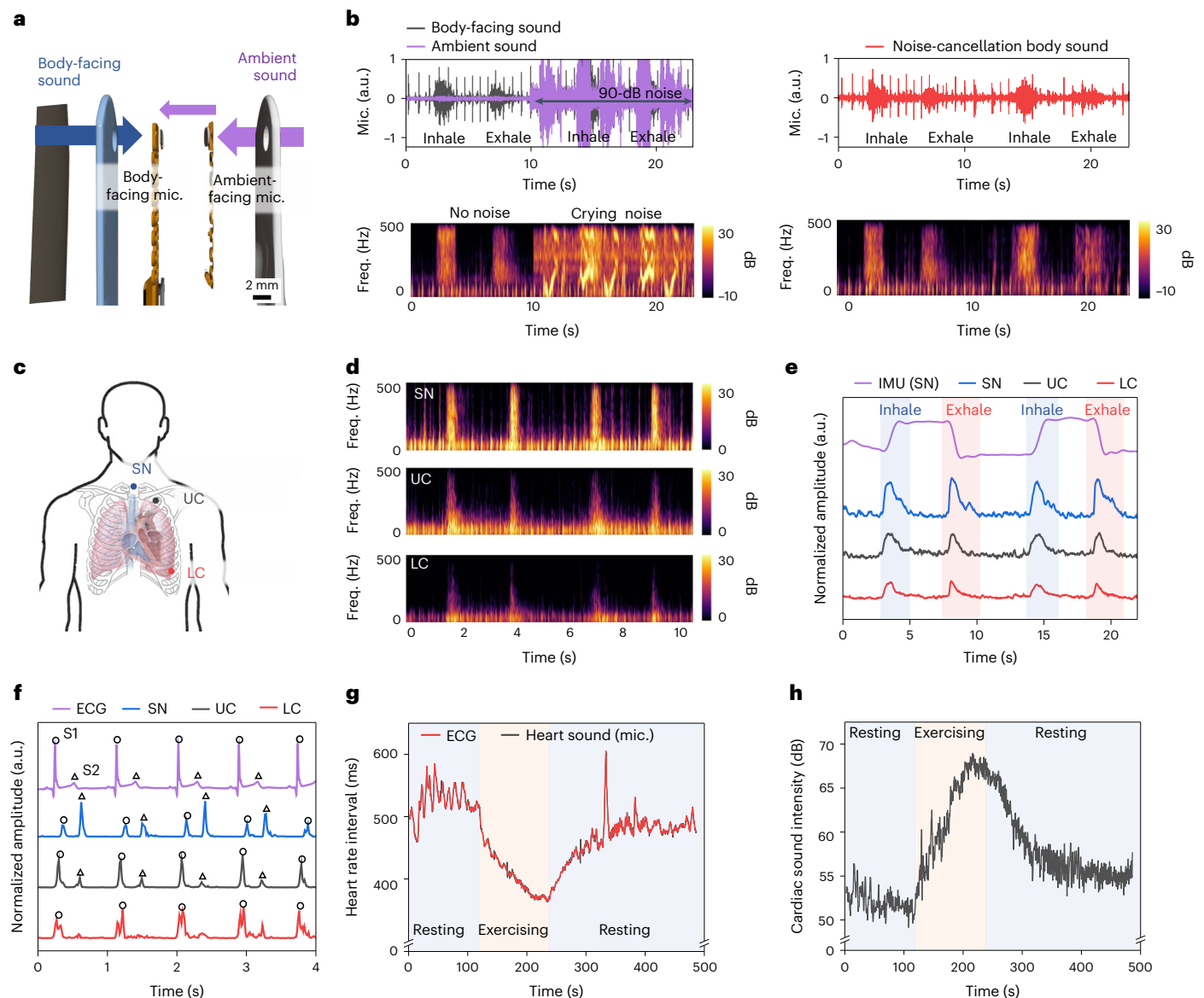
Fig. 2 | Characterization of individual BAMS systems and wireless networks for cardiorespiratory monitoring. a, Schematic illustration of the system for sound separation using a two-microphone setup. **b**, Examples of cardiorespiratory sounds from a healthy participant, captured in an ambient environment with white noise and with crying sounds at 90 dB. Shown are time-series data from the body- and ambient-facing microphones (top left), a spectrogram representation of time-series data from the body-facing microphone (bottom left) and corresponding results following two-step adaptive filtering (top and bottom right). Freq., frequency. **c**, Schematic illustration of body locations for cardiorespiratory monitoring. **d**, Example of a spectrogram of sounds from a healthy participant, collected on the suprasternal notch (SN), upper chest (UC) and lower chest (LC). **e**, Normalized data for chest wall movements of a healthy participant, extracted from the IMU of the device on the suprasternal notch, and sound intensity associated with respiration (respiratory sounds >150 Hz) at each location. **f**, Normalized ECG data and sound intensity, for a healthy participant, associated with cardiac activity (cardiac sounds <150 Hz) at each location. **g**, Comparison of heart rate interval between ECG and cardiac sounds of a healthy participant, derived from the microphone during a 2-min rest (2-min cycle exercise then 4-min rest). **h**, Cardiac sound intensity of a healthy participant while resting and exercising.

Adaptive algorithms for sound separation

As mentioned above, the body- and ambient-facing microphones capture sound information from two directions to enable differential detection of sounds from the body and its surroundings (Fig. 2a). A two-step adaptive filtering algorithm applied to the data recorded by these two microphones minimizes the contribution of ambient sounds to body sounds (Extended Data Fig. 2), and vice versa[26]. As an example, without this scheme, environments with crying sounds at 90 dB render detection of cardiopulmonary sounds impossible (Fig. 2b, left). Sound separation resolves this difficulty, as illustrated in spectrogram representations of data in Fig. 2b (right) for cardiopulmonary sounds and in audio reconstructions of data in Supplementary Video 1. Without separation,

the presence of 90-dB white noise, comparable to the sounds of a crying baby or subway noise, decreases the signal-to-noise ratio (SNR) of respiratory and cardiac sounds by >60% and nearly 50%, respectively (Extended Data Fig. 3); separation reduces this decrease to only 2 and 4%, respectively. This level of performance surpasses the 12 and 15% reduction, respectively, associated with the most widely used commercial digital stethoscope (3M Littmann CORE, Eko), which relies on a thick diaphragm and conventional active scheme for noise cancellation. In an environment with 90 dB of white noise, the sound-separated cardiac features extracted from the dual-microphone setup and seismocardiogram data captured by the IMU exhibited SNR values of 20 and 12 dB, respectively, in the case of a device mounted on the suprasternal notch. Both

results indicate negligible confounding effects of ambient sound (Supplementary Fig. 3). Application of the same separation algorithm to data from the ambient-facing microphone using data from the body-facing microphone yields sounds in the environment, with complementary value in understanding the context of patient care (Supplementary Fig. 4). This system can also be used in daily life scenarios where comprehensive monitoring of not only standard parameters such as heart rate and respiratory rate are possible, but also of autonomic measures including heart rate variability (HRV), cardiorespiratory coupling and swallowing, all with simultaneous measurements of body orientation and physical activity enabled by the IMU (Extended Data Fig. 4 and Supplementary Fig. 5). Moreover, the system operates well across various activities, encompassing sleep to exercise, providing high-quality data on physical activity levels, respiratory rate, respiratory sounds (frequency and intensity), heart rate and cardiac sound intensity over extended periods of time (Extended Data Fig. 5). The data collected during sleep also reveal patterns of snoring. Even during intense physical activity, the recordings allow for stable monitoring of respiratory and cardiac sounds. One shortcoming of these algorithms is in their inability to completely remove artifacts resulting from physical contact with the devices. Nevertheless the overall versatility and reliability of the system make it a promising tool for continuous and comprehensive health monitoring in diverse real-life situations (Supplementary Fig. 6).

Cardiorespiratory sounds with time-synchronized networks

Multiple devices can be operated simultaneously as the basis for spatial mapping of body sounds from different anatomical locations. For example, high-frequency tracheal and low-frequency vesicular sounds can be captured by recording from the suprasternal notch and chest area, respectively (Fig. 2d). Reduced speeds of airflow and increased movements of the lower chest wall lead to decreased intensity of respiratory sounds, defined as cumulative power spectral density >150 Hz following short-time Fourier transform (STFT) (Fig. 2e). The intensities of S1 cardiac sounds are higher than those of S2 on the lower chest, at locations close to the tricuspid and mitral valves of the heart. Conversely, the intensities of S2 sounds generated by the pulmonic and aortic valves are higher than those of S1 on the suprasternal notch (Fig. 2f). The S1 sound appears clearly in data from the lower chest, even during and after exercise, despite short R–R intervals (363 ms, heart rate 165 beats min^{-1} (bpm)). These intervals and the heart rates determined from the microphone data match those extracted from ECG recordings, with an average error of 0.2 ms and 0.02 bpm, thereby establishing the capacity for reliable measurement of HRV (Fig. 2g and Supplementary Fig. 7). These results are within the regulatory guidelines set by the US FDA (errors <±10% or ±5 bpm for heart rate). The Bland–Altman plot quantitatively compares the root mean square of continuous difference between cardiac cycles for HRV[27]. The average difference and standard deviation between root mean square of continuous difference values extracted from BAMS and ECG waveforms are 0.2 and 0.5 ms, respectively (Supplementary Fig. 8). Furthermore, the intensity of cardiac sounds, as depicted in Fig. 2h, increase during exercise. These sounds have the potential to correlate with blood pressure because they occur when a moving column of blood comes to a sudden stop or decelerates significantly. Comparison of the results from a blood pressure monitor (Finapres NOVA) with cardiac sound intensity reveal a high correlation trend (Supplementary Fig. 9), with Pearson's correlation coefficient = 0.83. The low-frequency nature of cardiac sounds (<150 Hz) provides clean separation from those associated with vocalization, enabling accurate cardiac activity monitoring in daily life scenarios such as exercising, walking and speaking, following sound separation (Supplementary Fig. 10).

Continuous monitoring of ambient and respiratory sounds in the NICU

Premature infants in the NICU are at risk of cardiorespiratory instability due to immature respiratory control centers and respiratory airflow obstruction, which typically manifest as central or obstructive apneas with fluctuations in heart rate and/or oxygen saturation[28–30]. Noise in the environment can further adversely affect these physiological responses, and excessive auditory stimulation can lead to additional risks of hearing loss and abnormal sensory responses[31]. As a result, continuous monitoring of both cardiopulmonary activity and noise characteristics local to the infant are important. Traditional methods for detection of airway obstruction, such as pneumotachography (pneumotach), capnography, nasal pressure or temperature measurements, are nonideal for continuous use due to (1) their bulky wired designs, (2) their sensitivity to artifacts associated with movements and basic operations in clinical care and (3) their incompatibility with nasal interfaces commonly used to provide noninvasive respiratory support in these infants. Additionally, levels of noise in the NICU room are seldom characterized or monitored. The technology introduced here addresses these shortcomings in a manner that is compatible with standard care practices.

Figure 3a highlights an example of the results of monitoring respiration from premature infants in an academic NICU. Figure 3b shows data from a pneumotach module, with simultaneous chest movements and sound recordings from a BAMS device on the suprasternal notch. Clear cardiac and respiratory signals appear in the spectrogram below and above 150 Hz, respectively. The pneumotach module detects adequate and reduced airflows, consistent with sound intensities observed in the spectrogram. Segments of absent airflow appear in both body sound and pneumotach measurements. Importantly, these periods of airflow obstruction are not consistently accompanied by absent movements of the chest. Several physiological reasons can explain these discrepancies. First, measurements of chest movements using accelerometry can be susceptible to noise caused by body motion. As a result, the amplitude of the chest movement signal does not necessarily equate with an equivalent and proportional change in lung volume during inspiration and expiration. Second, neonates are at risk of chest wall distortion due to their highly compliant chest wall. As a result, a rise in the chest movement signal indicates the presence of a respiratory effort but may not correlate with the degree of flow during that breath. Third, during brief periods of airflow limitation due to upper airway obstruction, infants continue to make respiratory efforts. For all those reasons, the magnitude of airflow and chest movement signals may not always correspond.

Figure 3c summarizes representative BAMS data from an in-NICU neonate, including ambient noise, body orientation, heart rate and respiratory rate, in comparison with readings obtained from FDA-approved clinical monitors (Supplementary Fig. 11). Both breathing interval and sound intensity, as determined by the BAMS device, correlate with pauses in breathing and breathing airflow rate. Supplementary Fig. 12 compares respiratory rates determined using pneumotach and body sounds for ten in-NICU neonates. The average difference and standard deviation of the respiratory rates were 0.44 and 2.13 bpm, respectively, a result lying within the range of FDA-cleared bedside monitoring systems (±3 bpm). The data for normalized airflow rates and respiratory sound intensities of ten in-NICU newborns show a Pearson's correlation value of 0.87 (Fig. 3d). Our findings reveal a high level of correlation values compared with those reported in previous studies (Supplementary Table 2). Additionally, Fig. 3e,f shows the distribution of breathing intervals and respiratory sound intensities of ten neonates over 500 s, showcasing the expected inter- and intra-variability in respiratory rates and airflow. Furthermore, the BAMS device reliably monitors respiratory sounds, heart rates and other physiological parameters over a prolonged period (3 h) in a cohort of five in-NICU neonates. The difference in heart rate determined using cardiac sounds and ECG waveforms is 0.015 bpm, with a standard deviation of 0.85 bpm (Extended Data Fig. 6). Respiratory sounds align well with chest movements, and also with data from respiratory inductance plethysmography and nasal temperature (Extended Data Fig. 7).
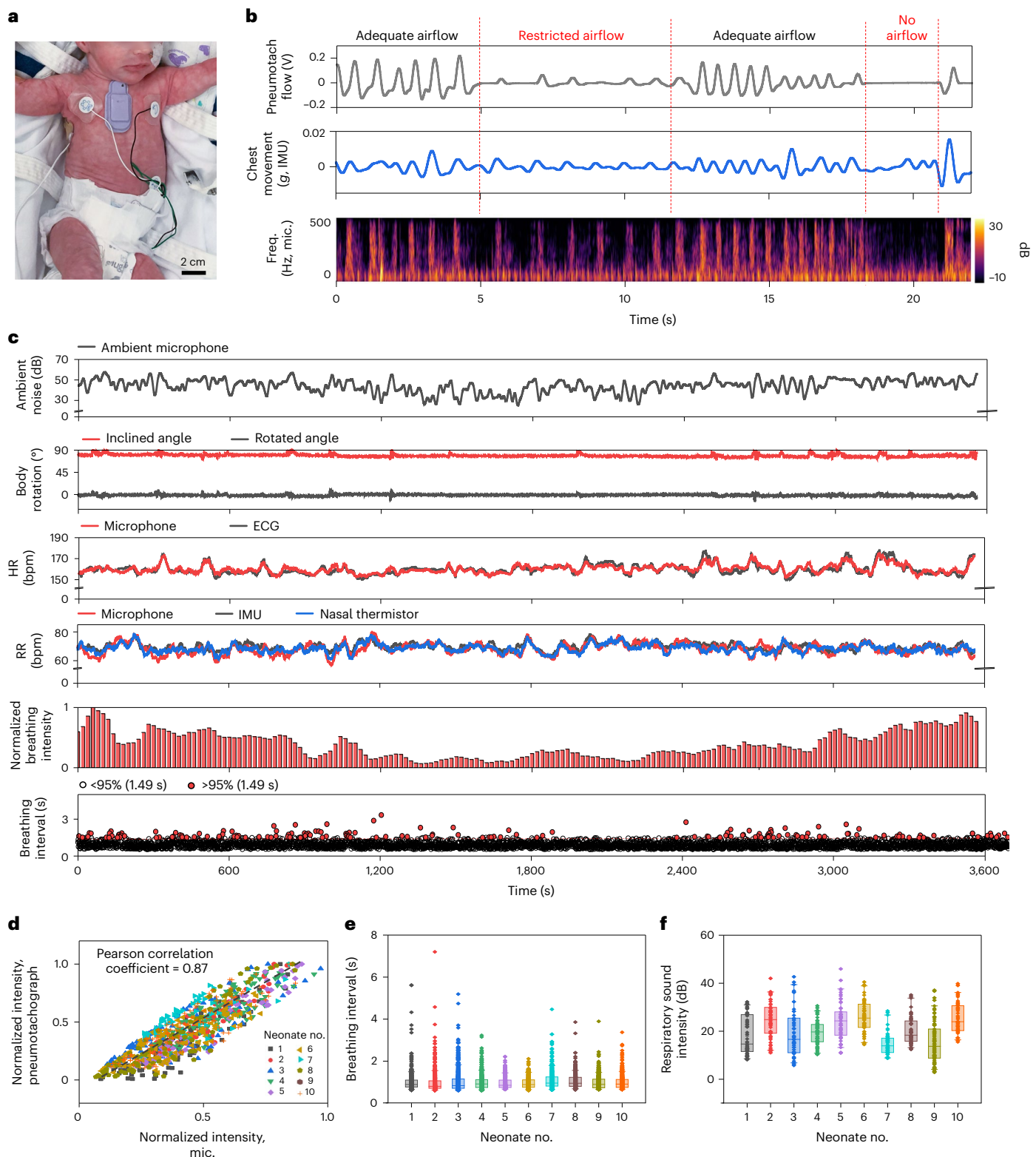
Fig. 3 | Continuous, wireless monitoring of respiratory sounds and other physiological parameters from neonates in a NICU. a, Photograph of BAMS device used on a neonate (born at 30-weeks gestation, 33-weeks postmenstrual age and weighing 1.56 kg). **b**, Representative respiration waveforms during different respiratory airflow conditions (adequate, restricted and no airflow) associated with a pneumotach device and with a BAMS system (chest movements and acoustic spectrograms) from a neonate. **c**, Ambient noise level, body rotation angle, heart rate (HR), respiratory rate (RR), normalized respiratory sound intensity and breathing intervals determined from data collected using a BAMS system and FDA-approved clinical monitors from a neonate. **d**, Plot showing the correlation between normalized intensity of pneumotach data and respiratory sounds from ten neonates (n = 61, 119, 103, 65, 98, 124, 55, 97, 90 and 100 data points for neonate nos. 1–10, respectively). **e,f**, Box plots showing breathing intervals (**e**) and respiratory sound intensity (**f**) recorded from ten neonates for 500 s (n = 619, 796, 1,154, 686, 747, 721, 737, 706, 677 and 636 data points for neonate nos. 1–10, respectively). Boxes show range between the 25th and 75th percentiles, whiskers show range between the 5th and 95th percentiles and midline indicates the median of each dataset.

The difference in respiratory rate determined by respiratory sounds and nasal temperature data is 0.06 bpm, with a standard deviation of 1.92 bpm (Extended Data Fig. 8). Moreover, the capabilities of the system can be extended by mounting two devices with time synchronization—one at the suprasternal notch and the other at the right upper chest—to investigate the movement of air through the trachea and the percentage of air transmitted to the lungs (Supplementary Fig. 13).

Spatiotemporal tracking of bowel sounds in the NICU

Sounds that result from the movement of food, gas and fluids during intestinal peristalsis provide valuable information on gastrointestinal health, of particular importance in the care of newborns in the NICU[32,33]. Tracking these bowel sounds can aid in diagnosis of intestinal motility disorders[34–36]. Our studies indicate a correlation between bowel sounds recorded by BAMS devices and electromyography signals from an adult's abdomen (Supplementary Fig. 14). Intestinal motility and its associated muscular contractions in the intestines lead to simultaneous bowel sounds and corresponding electromyography signals. Furthermore, the unique capabilities of time-synchronized networks of BAMS devices allow for long-term continuous monitoring of gastrointestinal sounds, which holds significant promise for studying and understanding the dynamics of intestinal peristalsis over extended periods.

Figure 4a displays such a system, attached to the right upper and left lower abdomen of an infant. Figure 4b,c shows spectrograms and sound intensities recorded from the right upper abdomen before and after feeding, respectively. The data-processing flow presented in Supplementary Fig. 15 identifies peaks in sound intensity that exceeded a certain threshold when accelerations associated with motion are <0.1g, to eliminate artifacts that can arise from physical contact with the device. The trends in normalized intensity and bowel sound peak counts captured from the right and left abdomen are shown in Fig. 4d. The difference in normalized intensities yields spatiotemporal information related to intestinal motility. The number of peaks in bowel sounds from three infants increases, from an average of five to 21 min^{-1}, before and after feeding, respectively (Fig. 4e). The average intensity in the right upper abdomen is 27.5 dB before feeding and 36.9 dB after (Fig. 4f). Post feeding, peaks are distributed mainly in the right upper quadrant of the abdomen for the first 15 min and then largely migrate to the left lower quadrant of the abdomen for the next 15 min (Fig. 4g). These results align with expectations based on measurements of adult bowel sounds using standard wire-based systems[34].

High-resolution, spatiotemporal mapping of lung

Strategies for wireless, time-synchronized operation of BAMS devices enable measurements with an average timing difference of 0.2 ms and standard deviation of 6 ms (Supplementary Fig. 16). This feature can be exploited to capture the distribution of lung sounds and body motions at many anatomical locations simultaneously so that the same breath may be analyzed across a range of lung regions. The results can enhance diagnosis and monitoring of various lung pathologies. The following pilot study utilizes 13 BAMS devices mounted on the anterior and posterior chest of 20 healthy participants and 35 patients with chronic lung disease, as depicted in Supplementary Fig. 17. Figure 5a and Supplementary Fig. 18 display computed tomography (CT) images of the lungs of a healthy participant (patient A) alongside spectrograms of sounds >150 Hz captured by the BAMS devices during inhalation and exhalation. Figure 5b and Supplementary Fig. 19 display corresponding results for a patient with chronic lung disease (radiation pneumonitis and fibrosis) and who, additionally, had undergone resection of their right upper lung lobe, part of their left upper lung lobe and right lower lung lobe (patient B). Data from patient A exhibit similar distributions of chest wall movement, maximum sound intensities and sound frequencies for the left and right sides of the body (Fig. 5c). The decrease in frequencies and intensities of sounds from the lower chest result from physiologically reduced rates of airflow and increased thickness of the chest wall.

Similar measurements performed on patients with chronic lung diseases and on patients who had undergone surgical lung resections reflect their condition. Patient B, with a history of resection surgery of the right upper and lower lobes and left upper lobe, shows decreased pulmonary function in the removed lobes, resulting in reduced airflow rates and lower sound intensity in the corresponding mapping (Fig. 5d, middle). Additionally, patient B's condition, with right peripheral pleuroparenchymal fibrosis, exhibits high-frequency and crackle sounds in the right lung, as seen in Fig. 5d (right) and Supplementary Fig. 20.

Figure 6 presents a comparative analysis of data obtained from healthy participants and patients with chronic lung diseases. This analysis highlights the significance of airflow rate, airflow volume and sound frequency in the diagnosis of obstructive and restrictive lung diseases. The results rely on data from BAMS devices mounted on the suprasternal notch and upper and lower posterior regions of the chest, along with separate measurements of nasal airflow rate and flow volume using a peak flow meter. During exhalation the airflow rate corresponds to the maximum sound intensity of cumulative power spectral density at 150 Hz and above. An additional parameter, sound energy, can be calculated by integration of sound intensity over time for comparison with nasal airflow volume (Supplementary Fig. 21). Figure 6a shows a correlation between sound intensity measured at different locations (suprasternal notch, upper posterior and lower posterior thorax) and nasal airflow rate for ten healthy participants. Pearson's correlation values between sound intensity and nasal airflow rate are 0.73, 0.79 and 0.75 at the suprasternal notch and upper and lower posterior positions, respectively. Similarly, correlation values between sound energy and nasal airflow volume are 0.71, 0.76 and 0.75 at these corresponding locations (Fig. 6b). Figure 6c illustrates the dominant frequency distribution of lung sounds in healthy participants at each location. This information is relevant in monitoring obstruction and airway conditions in patients with heterogeneous lung disease states. Specifically, as a marker of both airflow and volume, these parameters can assist with tracking of disease progression or response to treatment in patients with chronic lung diseases. Estimation of airflow rate and air volume can, additionally, facilitate monitoring of the Tiffeneau–Pinelli index, with the potential for daily monitoring of restrictive pulmonary diseases.

Figure 6d,f shows sound intensity measured at the suprasternal notch and the ratio of intensities from the left and right upper anterior chest for healthy participants, for patients with chronic lung diseases and no lung resections and for patients with right upper lobe or left upper lobe resection. Healthy participants exhibit higher sound intensity at the suprasternal notch than patients with chronic lung diseases, with an average intensity of 54 dB. In contrast, patients with chronic lung disease and no lung resections, those with left upper lung resections and those with right upper lung resections have average intensities of 38, 30 and 36 dB, respectively. Moreover, average sound intensity ratios (left upper lung sound intensity/right upper lung sound intensity) were 0.98, 1.01, 0.78 and 1.5, respectively, consistent with a reduction in sound intensities at the locations of resected lung tissues. Variations in this ratio exceed those attributable to uncertainties in attachment position, as depicted in Supplementary Fig. 22. Figure 6e,f compares the dominant expiratory frequency of the right upper posterior lung between healthy participants and those with chronic lung disease; the latter group exhibits an average frequency of 256 Hz. Healthy participants show frequencies of 219 Hz, distinguishing them from patients ($P < 0.05$). The onset of lung disease increases airway restrictions, thereby increasing the dominant sound frequency. Furthermore, sound intensity and frequency analyses conducted at diverse locations of the upper, middle and lower lobes of the lungs reveal marked differences between healthy participants and patients with chronic lung diseases, as presented in Supplementary Figs. 23 and 24.
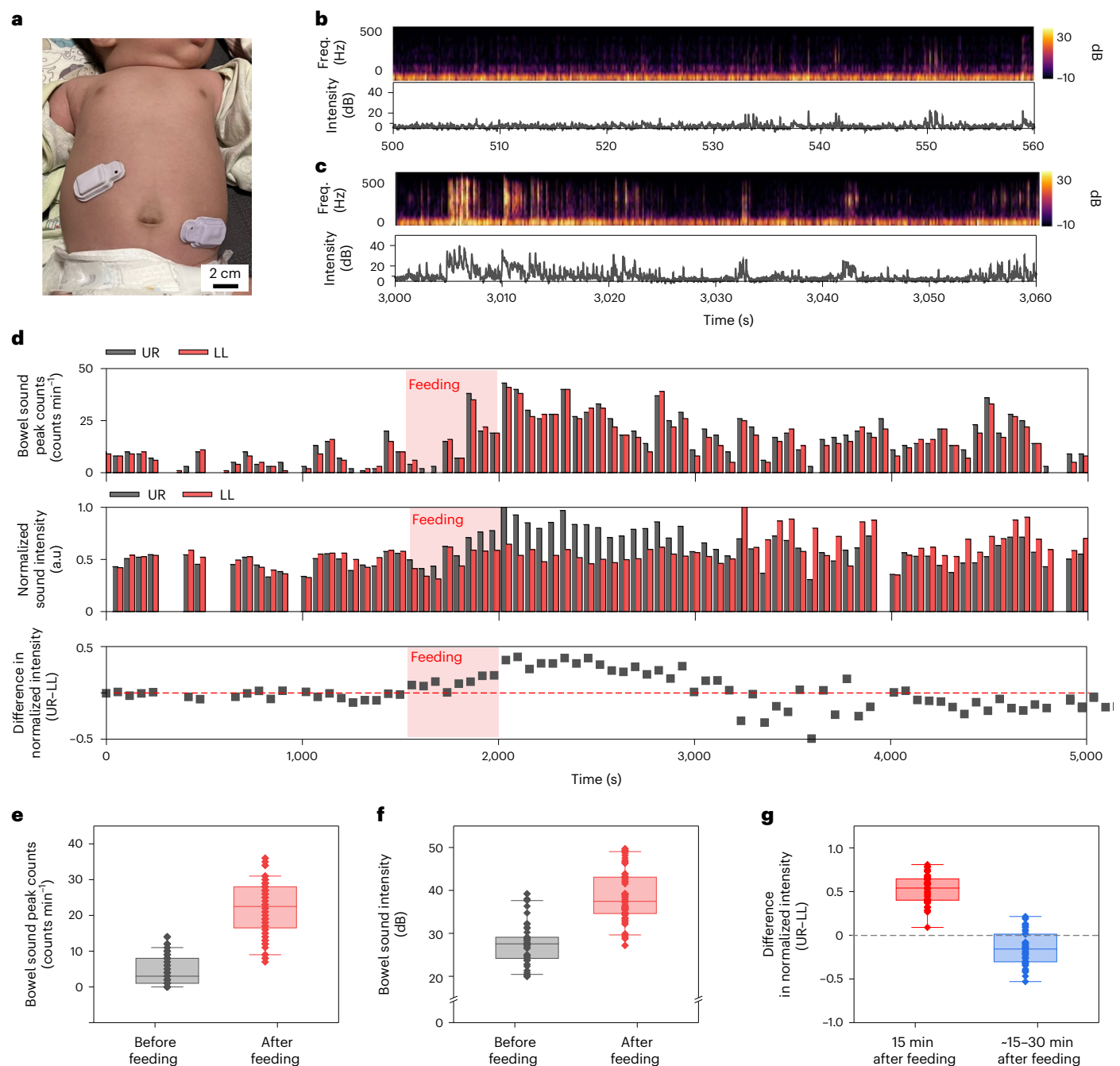
Fig. 4 | Continuous, wireless monitoring of gastrointestinal (bowel) sounds from neonates in a neonatal NICU. a, Photograph of a pair of BAMS devices applied to an infant (born at 38-weeks gestation, 46-weeks postmenstrual age and weighing 5.5 kg). **b,c**, Spectrograms and sound intensities (>150 Hz) for data collected before (**b**) and after feeding (**c**) using a BAMS system placed on the upper right abdomen of a neonate (born at 29-weeks gestation, 38-weeks postmenstrual age and weighing 2.6 kg). **d**, Bowel sound peak counts and normalized bowel sound intensity at the upper right (UR) and lower left abdomen (LL), and difference in normalized bowel sound intensity between UR and LL during tube feeding of the neonate. **e–g**, Box plots of bowel sound data from three neonates showing bowel sound peak counts min⁻¹ (**e**) ($n = 135$ and 216 data points for before and feeding, respectively), bowel sound intensity before and after feeding (**f**) ($n = 50$ and 142 data points for before and after feeding, respectively) and difference in normalized bowel sound intensity between the upper right and lower left abdomen 15 min after feeding and 15–30 min after feeding (**g**) ($n = 70$ and 76 data points for 15 min after feeding and for 15–30 min after feeding, respectively). Boxes show the range between the 25th and 75th percentiles, whiskers show the range between the 5th and 95th percentiles and midline indicates the median of each dataset.

Discussion

The present study introduces a technology designed for simultaneous measurement of body movements and sounds as a reliable source of physiological signals, with applicability both in the hospital and at home. Demonstration examples span from neonates with respiratory and digestive disorders in the NICU, to adult patients with lung disease in pulmonology clinics and to patients in the thoracic surgery clinic. Various characterization studies and performance-benchmarking measurements confirm the accuracy of the system and the uniqueness of its operational capabilities. The combination of two-microphone
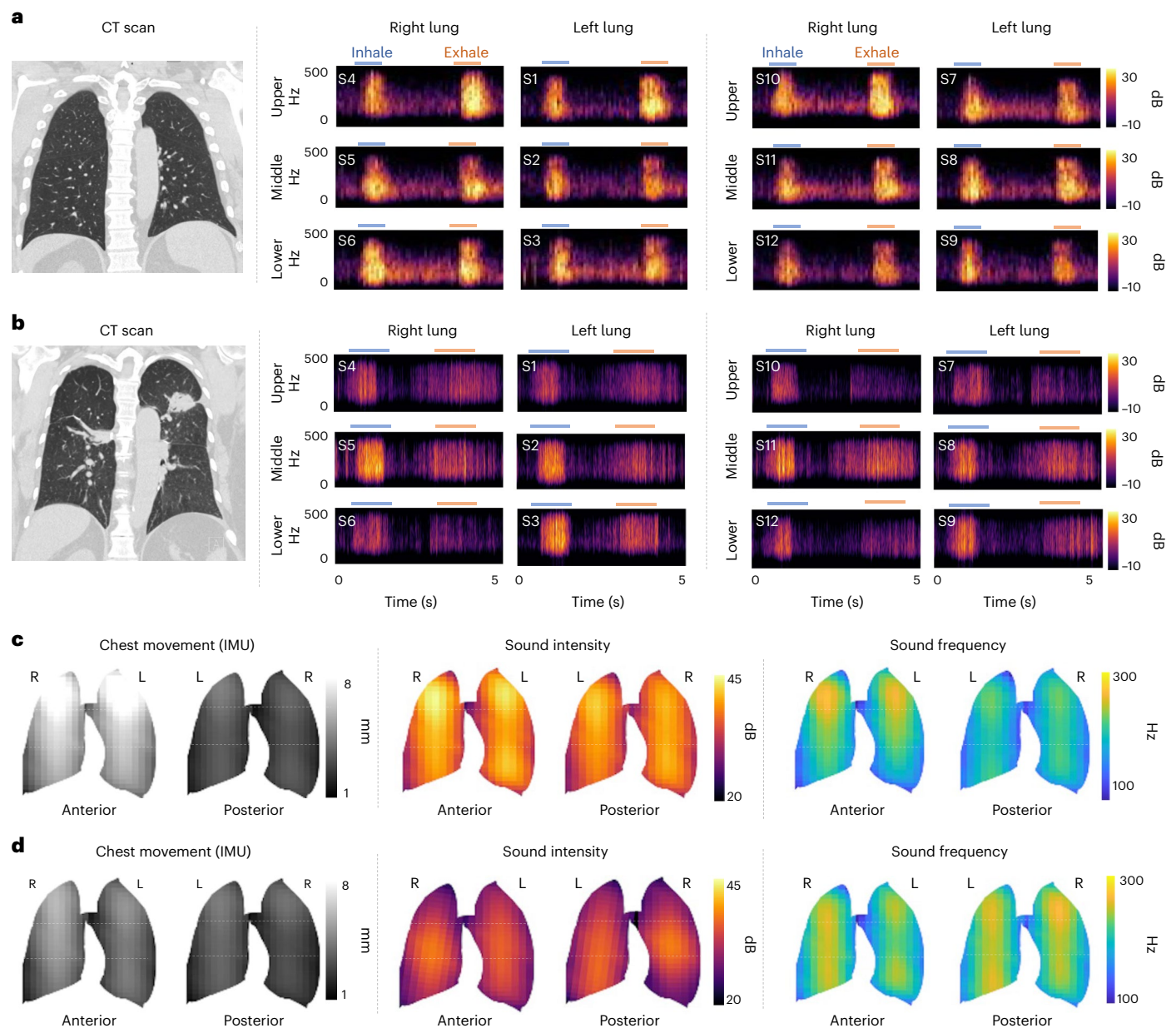
Fig. 5 | Wireless networks of BAMS systems and their use in simultaneous spatiotemporal mapping of lung sounds and chest wall movements.
a,b, CT image of lung (left) and sound distribution of the anterior lung (middle) and posterior lung (right) of a healthy participant (patient A) (**a**) and of a patient with chronic lung disease (patient B) (**b**). Data for the upper, middle and lower regions of the right and left lungs are shown. **c,d**, Distribution of chest movement (left), sound intensity (middle) and dominant sound frequency (right) of a healthy participant (**c**) and of a patient with lung disease (**d**) during exhalation. Data for anterior and posterior lung are shown.

design, sound-separation algorithms, broadband capabilities, time-synchronized operation of networks of devices and small, skin-compatible form create a broad range of unique possibilities in patient monitoring that deserve evaluation.

In the NICU, assessment of respiratory, cardiac and gastrointestinal sounds is an integral part of every aspect of nursing and medical care provided to all patients. The incorporation of BAMS devices into clinical practice offers the potential for continuous monitoring of these body sounds, facilitating decreased patient handling, reduced exposure to external vectors of infection and timely feedback in cases of physiological alterations[37–40]. When placed at the suprasternal notch, the BAMS device can detect both airflow and chest movements which, in combination, allow for the identification and classification of all apnea subtypes. Indeed, apneas are ubiquitous in

preterm infants and are a leading cause of in-hospital morbidities and prolonged NICU hospitalization yet cannot be accurately distinguished in terms of subtype using current monitoring standards. As such, enhanced apnea detection and classification in this population may lead to more targeted and personalized management approaches, improved patient outcomes and reduction in both length of hospitalization and costs. In addition, the BAMS system may aid in quantifying the degree of airflow obstruction in at-risk term neonates, such as infants with severe hypotonia (for example, trisomy 18, Prader–Willi Syndrome) and congenital upper airway obstruction (for example, Pierre Robin sequence). When placed simultaneously at the right and left anterior chest in mechanically ventilated neonates, resulting data can provide real-time feedback whenever air entry is diminished on one side relative to the other; this may promptly alert the clinician of a
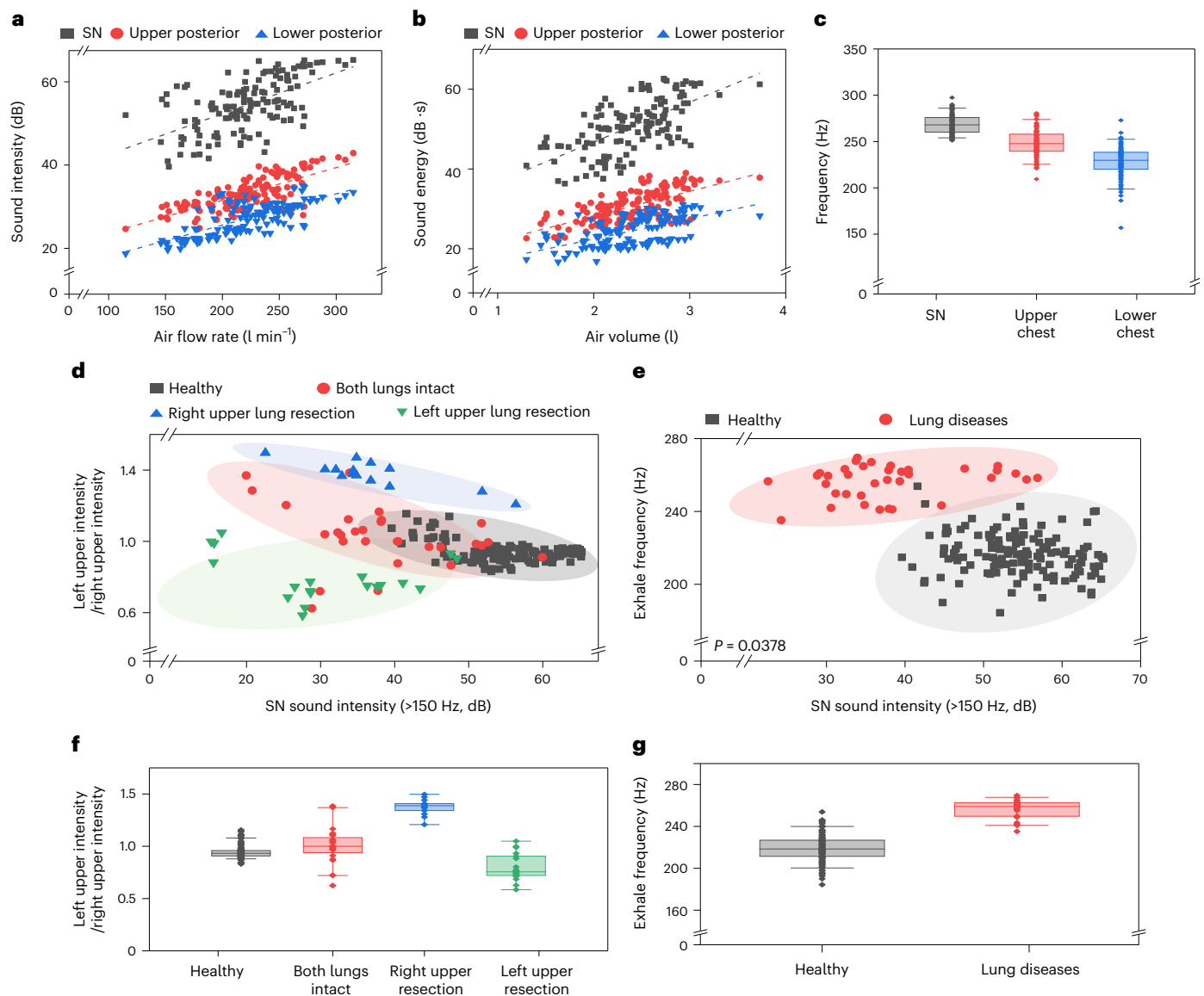
Fig. 6 | Analysis of the distribution of lung sounds across healthy participants and patients with chronic lung disease. a,b, Correlations of lung sound intensity and airflow rate (**a**) and of lung sound energy and air volume (**b**) from BAMS systems located on the suprasternal notch and upper and lower posterior chest for ten healthy participants (*n* = 137 data points each for suprasternal notch, upper posterior chest and lower posterior chest). **c,** Dominant frequency of lung sounds at the suprasternal notch, upper chest and lower chest during exhalation for ten healthy participants (*n* = 132 data points each for suprasternal notch, upper posterior chest and lower posterior chest). **d,** Distributions of the ratio of upper right and upper left anterior chest lung sound intensity and at the suprasternal notch during exhalation for healthy participants (20 participants, 138 data points), for patients with lung disease but with both lungs intact (eight patients, 25 data points) and for patients with lung disease involving either left upper lung resection (eight patients, 19 data points) or right upper lung resection (seven patients, 14 data points). **e,** Distributions of

right upper posterior dominant expiratory frequency and sound intensity at the suprasternal notch during exhalation in patients with disease in the right upper lung (13 patients, 36 data points) and in healthy participants without lung disease (20 participants, 138 datapoints). **f,** Box plot showing the ratio of lung sound intensity between the upper right and upper left anterior chest for healthy participants (20 participants, 138 data points), patients with lung disease but with both lungs intact (eight patients, 25 data points) and patients with lung disease involving either left upper lung resection (eight patients, 19 data points) or right upper lung resection (seven patients, 14 data points. **g,** Box plot showing dominant expiratory frequency in the upper posterior region of the right lung in patients with disease in the right upper lung (13 patients, 36 data points) and in participants without lung disease (20 participants, 138 data points). Boxes show range between the 25th and 75th percentiles, whiskers the range between the 5th and 95th percentiles and midline indicates the median of each dataset.

potential pathology such as atelectasis, consolidation or pneumothorax, thereby leading to early diagnosis and treatment. When placed at different quadrants of the abdomen, reduced bowel sounds may act as an early warning sign for impending gastrointestinal complication such as bowel dysmotility, obstruction or necrotizing enterocolitis. In contrast, increasing bowel sounds may serve as objective markers of improved peristalsis and bowel health following gastrointestinal surgery, thereby aiding in the decision to resume or progress feeds.

The advanced assessment of lung health presents a significant opportunity in this study. Traditional auscultation using a stethoscope demands considerable expertise and time, often leading to rushed examinations that may result in inaccuracies and delays in providing appropriate diagnostic workups and treatments[41–43]. Moreover, standard pulmonary function tests offer a single numeric value, assuming equal contribution from all lung regions, a premise disproven in chronic lung disease. In contrast, the technology introduced here

can be employed either independently or in tandem with pulmonary function tests, offering real-time insights into regional lung function and disease status. This capability will prove invaluable in postoperative management of lung resection, enabling daily monitoring to track regional lung recovery and promptly address any complications, ultimately elevating the standard of medical care. Additionally, BAMS devices serve as a crucial tool in the intensive care unit, assisting providers in optimization of ventilator settings by providing real-time feedback on regional lung ventilation. Given the current lack of portable diagnostic tools, the ability to conduct real-time regional lung function assessments at the bedside is of paramount importance because transfer of patients for additional tests can pose risks.

Additional possibilities, examined but not systematically explored in the results presented here, include monitoring of swallowing events and respiratory cycles for patients with dysphagia, tracking of patterns of speech for patients with dementia and measuring a collection of parameters, including HRV, related to cardiorespiratory function for patients with diabetes, high blood pressure, cardiac arrhythmias, asthma, anxiety and depression. Such measurements have the potential not only to enhance clinical decision making but also to improve patient comfort and reduce the burden on healthcare facilities. The results serve as a foundation for development in the field of physiological monitoring, opening up possibilities for the future of healthcare.

Online content

References

1. Virani, S. S. et al. Heart Disease and Stroke Statistics–2020 Update: a report from the American Heart Association. *Circulation* **141**, e139–e596 (2020).
2. Rajaratnam, J. K. et al. Neonatal, postneonatal, childhood, and under-5 mortality for 187 countries, 1970–2010: a systematic analysis of progress towards Millennium Development Goal 4. *Lancet* **375**, 1988–2008 (2010).
3. Choi, Y. S. et al. A transient, closed-loop network of wireless, body-integrated devices for autonomous electrotherapy. *Science* **376**, 1006–1012 (2022).
4. Jeong, H. et al. Differential cardiopulmonary monitoring system for artifact-canceled physiological tracking of athletes, workers, and COVID-19 patients. *Sci. Adv.* **7**, eabg3092 (2021).
5. Kaszala, K. & Ellenbogen, K. A. Device sensing: sensors and algorithms for pacemakers and implantable cardioverter defibrillators. *Circulation* **122**, 1328–1340 (2010).
6. Liu, C. et al. Wireless, skin-interfaced devices for pediatric critical care: application to continuous, noninvasive blood pressure monitoring. *Adv. Healthc. Mater.* **10**, e2100383 (2021).
7. Chung, H. U. et al. Binodal, wireless epidermal electronic systems with in-sensor analytics for neonatal intensive care. *Science* **363**, eaau0780 (2019).
8. Chung, H. U. et al. Skin-interfaced biosensors for advanced wireless physiological monitoring in neonatal and pediatric intensive-care units. *Nat. Med.* **26**, 418–429 (2020).
9. Wang, M. et al. A wearable electrochemical biosensor for the monitoring of metabolites and nutrients. *Nat. Biomed. Eng.* **6**, 1225–1235 (2022).
10. Boriosi, J. P., Zhao, Q., Preston, A. & Hollman, G. A. The utility of the pretracheal stethoscope in detecting ventilatory abnormalities during propofol sedation in children. *Paediatr. Anaesth.* **29**, 604–610 (2019).
11. Du, X., Allwood, G., Webberley, K. M., Osseiran, A. & Marshall, B. J. Bowel sounds identification and migrating motor complex detection with low-cost piezoelectric acoustic sensing device. *Sensors* **18**, 4240 (2018).
12. Jahin, S., Moniruzzaman, M., Alvee, F. M., Haque, I. U. & Kalpoma, K. A. A modern approach to AI assistant for heart disease detection by heart sound through created e-Stethoscope. In *2022 25th International Conference on Computer and Information Technology (ICCIT)* 669–674 (IEEE, 2022).
13. Kölle, K., Aftab, M. F., Andersson, L. E., Fougner, A. L. & Stavdahl, Ø. Data driven filtering of bowel sounds using multivariate empirical mode decomposition. *Biomed. Eng. Online* **18**, 28 (2019).
14. Lee, S. H. et al. Fully portable continuous real-time auscultation with a soft wearable stethoscope designed for automated disease diagnosis. *Sci. Adv.* **8**, eabo5867 (2022).
15. Pasterkamp, H. The highs and lows of wheezing: a review of the most popular adventitious lung sound. *Pediatr. Pulmonol.* **53**, 243–254 (2018).
16. Sharma, P., Imtiaz, S. A. & Rodriguez-Villegas, E. Acoustic sensing as a novel wearable approach for cardiac monitoring at the wrist. *Sci. Rep.* **9**, 20079 (2019).
17. Zhou, L. et al. Acoustic analysis of neonatal breath sounds using digital stethoscope technology. *Pediatr. Pulmonol.* **55**, 624–630 (2020).
18. Jeong, H. et al. Closed-loop network of skin-interfaced wireless devices for quantifying vocal fatigue and providing user feedback. *Proc. Natl Acad. Sci. USA* **120**, e2219394120 (2023).
19. Kang, Y. J. et al. Soft skin-interfaced mechano-acoustic sensors for real-time monitoring and patient feedback on respiratory and swallowing biomechanics. *NPJ Digit. Med.* **5**, 147 (2022).
20. Lee, K. et al. Mechano-acoustic sensing of physiological processes and body motions via a soft wireless device placed at the suprasternal notch. *Nat. Biomed. Eng.* **4**, 148–158 (2020).
21. Chowdhury, M. E. et al. Real-time smart-digital stethoscope system for heart diseases monitoring. *Sensors* **19**, 2781 (2019).
22. Islam, M. A., Bandyopadhyaya, I., Bhattacharyya, P. & Saha, G. Multichannel lung sound analysis for asthma detection. *Comput. Methods Progr. Biomed.* **159**, 111–123 (2018).
23. Rao, A., Ruiz, J., Bao, C. & Roy, S. Tabla: a proof-of-concept auscultatory percussion device for low-cost pneumonia detection. *Sensors* **18**, 2689 (2018).
24. Shimoda, T. et al. Lung sound analysis helps localize airway inflammation in patients with bronchial asthma. *J. Asthma Allergy* **10**, 99–108 (2017).
25. Wang, F. et al. A flexible skin-mounted wireless acoustic device for bowel sounds monitoring and evaluation. *Sci. China Inf. Sci.* **62**, 202402 (2019).
26. Vanden Berghe, J. & Wouters, J. An adaptive noise canceller for hearing aids using two nearby microphones. *J. Acoust. Soc. Am.* **103**, 3621–3626 (1998).
27. Bland, J. M. & Altman, D. Statistical methods for assessing agreement between two methods of clinical measurement. *Lancet* **327**, 307–310 (1986).
28. Dipietro, J. A., Caughy, M. O. B., Cusson, R. & Fox, N. A. Cardiorespiratory functioning of preterm infants: stability and risk associations for measures of heart rate variability and oxygen saturation. *Dev. Psychobiol.* **27**, 137–152 (1994).
29. Hasenstab, K. A., Nawaz, S., Lang, I. M., Shaker, R. & Jadcherla, S. R. Pharyngoesophageal and cardiorespiratory interactions: potential implications for premature infants at risk of clinically significant cardiorespiratory events. *Am. J. Physiol. Gastrointest. Liver Physiol.* **316**, G304–G312 (2019).

30. Ludington-Hoe, S., Anderson, G. C., Swinth, J., Thompson, C. & Hadeed, A. Randomized controlled trial of kangaroo care: cardiorespiratory and thermal effects on healthy preterm infants. *Neonatal Netw.* **23**, 39–48 (2004).

31. Wachman, E. M. & Lahav, A. The effects of noise on preterm infants in the NICU. *Arch. Dis. Child. Fetal Neonatal Ed.* **96**, F305–F309 (2011).

32. Inderjeeth, A.-J., Webberley, K. M., Muir, J. & Marshall, B. J. The potential of computerised analysis of bowel sounds for diagnosis of gastrointestinal conditions: a systematic review. *Syst. Rev.* **7**, 124 (2018).

33. Tomomasa, T. et al. Gastrointestinal sounds and migrating motor complex in fasted humans. *Am. J. Gastroenterol.* **94**, 374–381 (1999).

34. Chien, C.-H., Huang, H.-T., Wang, C.-Y. & Chong, F.-C. Two-dimensional static and dynamic display system of bowel sound magnitude map for evaluation of intestinal motility. *Biomed. Eng. Appl. Basis Commun.* **21**, 333–342 (2009).

35. Li, B., Wang, J.-R. & Ma, Y.-L. Bowel sounds and monitoring gastrointestinal motility in critically ill patients. *Clin. Nurse Spec.* **26**, 29–34 (2012).

36. Nowak, J. K., Nowak, R., Radzikowski, K., Grulkowski, I. & Walkowiak, J. Automated bowel sound analysis: an overview. *Sensors* **21**, 5294 (2021).

37. O'Flaherty, N. & Fenelon, L. The stethoscope and healthcare-associated infection: a snake in the grass or innocent bystander? *J. Hosp. Infect.* **91**, 1–7 (2015).

38. Wright, I., Orr, H. & Porter, C. Stethoscope contamination in the neonatal intensive care unit. *J. Hosp. Infect.* **29**, 65–68 (1995).

39. Youngster, I., Berkovitch, M., Heyman, E., Lazarovitch, Z. & Goldman, M. The stethoscope as a vector of infectious diseases in the paediatric division. *Acta Paediatr.* **97**, 1253–1255 (2008).

40. Guilleminault, C. & Pelayo, R. Sleep-disordered breathing in children. *Ann. Med.* **30**, 350–356 (1998).

41. Pasterkamp, H., Kraman, S. S. & Wodicka, G. R. Respiratory sounds: advances beyond the stethoscope. *Am. J. Respir. Crit. Care Med.* **156**, 974–987 (1997).

42. Wilkins, R. L. Is the stethoscope on the verge of becoming obsolete? *Respir. Care* **49**, 1488–1489 (2004).

43. Arts, L., Lim, E. H. T., van de Ven, P. M., Heunks, L. & Tuinman, P. R. The diagnostic accuracy of lung auscultation in adult patients with acute pulmonary pathologies: a meta-analysis. *Sci. Rep.* **10**, 7347 (2020).

¹Querrey Simpson Institute for Bioelectronics, Northwestern University, Evanston, IL, USA. ²Division of Electrical Engineering, Hanyang University ERICA, Ansan, Republic of Korea. ³Neonatal Division, Department of Pediatrics, McGill University Health Center, Montreal, Quebec, Canada. ⁴Division of Thoracic Surgery, Department of Surgery, Feinberg School of Medicine, Northwestern University, Chicago, IL, USA. ⁵School of Electrical Engineering, Korea Advanced Institute of Science and Technology, Daejeon, Republic of Korea. ⁶Department of Polymer Science and Engineering, Dankook University, Yongin, Republic of Korea. ⁷Department of Electrical and Computer Engineering, University of California, Davis, CA, USA. ⁸Department of Electrical and Computer Engineering, Northwestern University, Evanston, IL, USA. ⁹Adlai E. Stevenson High School, Lincolnshire, IL, USA. ¹⁰Department of Advanced Materials Engineering for Information and Electronics, Kyung Hee University, Gyeonggi-do, Republic of Korea. ¹¹Sibel Health, Niles, IL, USA. ¹²Department of Pediatrics, Northwestern University Feinberg School of Medicine, Chicago, IL, USA. ¹³Division of Autonomic Medicine, Department of Pediatrics, Ann & Robert H. Lurie Children's Hospital of Chicago, Chicago, IL, USA. ¹⁴Stanley Manne Children's Research Institute, Chicago, IL, USA. ¹⁵These authors contributed equally: Jae-Young Yoo, Seyong Oh, Wissam Shalish, Woo-Youl Maeng. ✉e-mail: ankit.bharat@nm.org; jrogers@northwestern.edu

Methods

Fabrication of BAMS devices

Each device included five components: a pair of microphones, an IMU, flash memory, Bluetooth SoC and hardware for power and wireless charging. Locating the first two components on separate islands with serpentine traces as interconnects enhanced the mechanical deformability of the system. The ambient- and body-facing microphones (ICS-40180, TDK) were each connected to an amplifier circuit with 64-fold gain and a bandpass filter ranging from 10 Hz to 2 kHz. The amplified signal was converted to a 14-bit analog-to-digital converter value at a sampling rate of 1 kHz. The IMU (LSM6DSL, STMicroelectronics) delivered three-axis acceleration data at a sampling rate of 104 Hz to the Bluetooth SoC (ISP-1807, Insight SIP) via serial peripheral interface communication protocols. The microphone data at 1 kHz and IMU data at 104 Hz were passed into 2-GB flash memory (MT29F2G, Micron) with time stamps defined using an internal clock at 16 MHz. By utilization of 2-GB flash memory we are able to store data in the local memory for up to 16 h. For continuous monitoring over periods >16 h we can transfer data in real time to an iPad/iPhone placed nearby; local memory can then be used for data storage during other times (Supplementary Fig. 25). The wireless-charging and power components included a charging coil with a resonance frequency of 13.56 MHz, a voltage rectifier, a voltage regulator, a battery charger integrated circuit and a 3.7-V lithium-polymer battery (110 mAh). Customized firmware was uploaded to the Bluetooth SoC using Segger Embedded Studio. A silicone elastomer (Silbione-4420) defined an encapsulating structure with overall dimensions of 40 × 20 mm², thickness 8 mm and weight 6 g.

Wireless-charging system

Our BAMS system incorporates a wireless-charging scheme that operates at a standard radio frequency band of 13.56 MHz and that is approved by the Federal Communications Commission for use in industrial, scientific and medical devices. This frequency band was chosen for its minimal absorption in living tissues, ensuring the safety and wellbeing of the user during charging[44]. During routine use the BAMS device is removed from the body for charging, ensuring a convenient and hassle-free charging experience. However, in certain demanding situations where continuous monitoring is crucial, such as with infants, the device can be considered for charging while still being worn by the baby. To assess the safety and efficacy of in situ charging, we conducted tests using an infant model and monitored the temperature during an 8-h charging period using an infrared camera (FLIR ONE pro, FLIR, Inc.). The results showed that the temperature difference between the device and the ambient environment was consistently maintained within 0.5 °C throughout the charging process (Supplementary Fig. 26). This temperature stability demonstrates the safe and controlled charging performance of the BAMS device, ensuring that it remains well within the acceptable temperature range for use with infants.

Characterization of body- and ambient-facing microphones

Experiments with white noise (frequencies ranging 20–400 Hz) and a commercial sound meter in a soundproof radiofrequency room served as the basis for characterization of the performance of the microphones. A linear fitting process calibrated the decibels of white noise to sound intensity, measured as the integration of power spectral density from 20 to 400 Hz associated with STFT of the microphone data (Supplementary Fig. 4).

Tests of sound-separation algorithms using two-step adaptive filtering involved a BAMS device and a commercial digital stethoscope (3M Littmann CORE, Eko) with active noise cancellation mounted on a lung sound trainer to produce constant breath and lung sounds. Measurements examined the effects of the decibel level of various types of noise source. In the presence of 90-dB white noise (frequencies 20–400 Hz), the SNR of respiratory and cardiac sounds captured using the commercial digital stethoscope decreased by 12 and 15%,

respectively; without sound separation in the BAMS device, SNR decreased by 62 and 48%, respectively (Extended Data Fig. 3) although, with separation, the reduction in SNR was only 2 and 4%, respectively, for the BAMS device.

Time-synchronized network system

The scheme for time synchronization between multiple devices exploited a master device to broadcast its 16-MHz local clock information through radiofrequency signals at 100-ms intervals to slave devices with different radiofrequency addresses. Updates to the local clock information of the slave devices used the clock information received from the master. This clock information was also passed to the mobile device for storage in memory with the coordinated universal time.

Characterization of the accuracy of this scheme involved monitoring peak delay among 13 devices exposed to sound swept from 500 Hz to 1 kHz sourced from a vibration generator at a speed of 5 Hz s⁻¹. Cross-correlation of time-series sound data defined time delays between each device. The results showed an average timing difference of 0.2 ms and a standard deviation of 6 ms (Supplementary Fig. 16). During on-body testing, a master device was placed next to the monitoring iPad to transmit accurate time information. We attached 13 BAMS devices to the chest and back of the body, with these receiving time information from the master through radiofrequency communication. To assess time synchronization errors, sound from an external metronome was used to calculate the time differences of sound peaks recorded by each sensor. The results, as shown in Supplementary Fig. 27, revealed an average time difference of 0.4 ms and maximum time difference of 6 ms over a duration of 150 min. With Bluetooth 5 standards used in recent iPhone and iPad models, it is possible to connect and control more than 30 Bluetooth devices simultaneously. This capability allowed us to control time-synchronized devices simultaneously through a graphical user interface. To minimize communication load on the control iPad, which connects all 13 sensors, we stored the data in local flash memory rather than streaming them in real time.

Sound separation

Data collected from the body- and ambient-facing microphones included contributions from both body and ambient sounds. Sound separation used a two-step adaptive filtering method, as depicted in Extended Data Fig. 2. In the first adaptive filtering, the ambient sound noise signal is extracted by subtracting the body-facing microphone's sound signal from that of the ambient-facing microphone. In the second adaptive filtering, the body sound signal is obtained by subtracting the ambient sound noise signal, extracted by the first adaptive filtering, from that of the body-facing microphone. These processes use the recursive least-squares adaptive filter provided in MATLAB at each adaptive filtering step. Recursive least-squares filtering parameters involve a filter length of ten taps and a forgetting factor of 0.98.

To verify the effectiveness of sound separation, a validation experiment was conducted using respiratory sound measurements. Initially, respiratory sounds were recorded on the lung sound trainer (Simulaids, Nasco Education) for 24 s without any ambient noise, as illustrated in Extended Data Fig. 9a. Subsequently respiratory sound measurements were continued, this time with the addition of 70-dB white noise. When examining the frequency distribution of respiratory sounds without ambient noise, a relatively even distribution was observed >150 Hz, as shown in Extended Data Fig. 9b. However, when ambient sound noise >150 Hz was present, it significantly distorted respiratory sound signals. Even following the application of bandpass filtering within the range 150–300 Hz, where respiratory sounds are relatively strong, respiratory sound signals remained unclear due to the presence of ambient noise (Extended Data Fig. 9c). Respiratory sound intensity between 150 and 300 Hz exhibited a SNR of 27 dB without ambient noise, but this decreased to 17 dB in the presence of 70-dB ambient noise. However, the sound-separation techniques employed in the BAMS device

effectively separated respiratory sound signals from ambient noise, as demonstrated in Extended Data Fig. 9d. Clear respiratory sound signals were observed on the spectrogram even in the presence of ambient noise following application of the sound-separation process. The SNR of sound intensity was maintained at 26 dB.

Cardiorespiratory sound analysis

Data were processed using a two-step adaptive filtering method and subjected to both low- and high-pass filtering (third order, with an attenuation rate of −58 dB per decade) and cutoff frequency of 150 Hz. This filtering process effectively distinguished between respiratory and cardiac sounds based on their frequency characteristics. The analysis revealed that 76% of the total signal for respiratory sounds exists >150 Hz while 81% of the total signal for cardiac sounds exists <150 Hz (Supplementary Fig. 28). STFT yielded power spectral density information for each frequency of the filtered signal, with a window size of 0.03 s and overlap length of 0.027 s. Respiratory sound intensity values followed from integration of power spectral density across frequencies >150 Hz. Similar data for cardiac sounds followed from integration of power spectral density associated across frequencies ranging 20–150 Hz. Respiratory and cardiac sound intensity data were then used to identify peaks in respiratory and cardiac cycles. For calculation of respiratory rate, intensity peaks corresponding to inhalation and exhalation events were identified on the respiratory sound intensity graph. Chest movement data were used to distinguish between inhalation and exhalation during the detection of each sound intensity peak. Respiratory rate was then calculated by selecting the maximum value between the count of inhalation and exhalation sound peaks over a 60-s period. This approach prevents the underestimation of respiratory rate caused by the overlap of inhalation and exhalation sounds at high respiratory rates (Supplementary Fig. 29).

For body orientation analysis, the thre-axis acceleration signal obtained from the IMU was filtered using a Butterworth low-pass filter (third order) with a cutoff frequency of 0.1 Hz. Body orientation was calculated from the filtered signals by simple trigonometry. Additionally, the chest movement signal was obtained by applying a bandpass filter (third order) with frequency range 0.1–1 Hz. The chest movement signal correlated well with respiratory sounds detected from the microphone, even under low-frequency movements such as resting (near 0-Hz movement), walking (0.8-Hz movement) and squatting (0.2-Hz movement) (Supplementary Fig. 30). Physical activity levels were monitored using the root mean square of acceleration values along the x, y and z axes, processed with a Butterworth bandpass filter (third order) at 1–10 Hz.

Bowel sound analysis

Data were processed using a two-step adaptive filtering method with a bandpass filtered between 150 and 400 Hz to eliminate heart sound. A STFT of the filtered signal, with a window size of 0.03 s and overlap length of 0.027 s, yielded power spectral density. Integration of these data for frequencies >150 Hz yielded bowel sound intensity data. Sound peaks of width <100 ms and intensity >20 dB were then identified. To eliminate signals that can result from movements or physical contacts with the device, only features during periods of physical activity (accelerations from the IMU) of magnitude <0.1g were included in the identification of bowel sound peaks.

Device mounting

A medical-grade adhesive (2477P, 3M Medical Materials & Technologies) was used as the interface between BAMS and the skin; this product is widely recognized and approved for use in the context of bandages (ISO 10993-5), and for the fragile skin of preterm infants. This adhesive allowed for reliable and secure fixation of the device to the infants in this study (median gestational age 28 weeks (minimum 25 to maximum 31 weeks)) and a median postmenstrual age of 35 weeks (minimum 33 to maximum 36 weeks), with no adverse skin reactions

during placement or following removal of the sensors. Furthermore, we previously reported on a slightly larger wireless wearable device using the same adhesive in a cohort of 50 neonates of gestational age 23–40 weeks and postnatal age 1 week to 4 years, with no instances of skin breakdown or dermatitis (as graded by a certified dermatologist)[8]. Furthermore, these silicone-based adhesives also conform rapidly and readily to uneven surfaces, which makes them practical for use in infants with limited space options for placement of the sensor (Supplementary Fig. 31). The microphone collects data from the skin through the bottom layer, polyimide film and adhesive. We used a thickness of 0.3 mm for the bottom layer, 50 µm for the polyimide film and 0.5 mm for the adhesive, to achieve high sensitivity in capture of acoustic signals in placing the sensor close to the body (Supplementary Fig. 32).

Clinical tests

The study protocol was approved by the Northwestern Medicine Institutional Review Board (no. STU00218021) and the McGill University Health Center Research Ethics Board (no. IRB00010120). Informed consent was obtained from all participants or their guardians. Trained research staff placed BAMS devices on participants in a location that did not interfere with clinical monitoring equipment. Monitoring in the NICU included ECG, nasal temperature, chest and abdomen movements using respiratory inductance plethysmography, and a pneumotachograph device. Research staff recorded additional information such as clinical data, infant movement and fussing during data collection. For the lung sound study in patients, the research staff attached 13 devices to the anterior and posterior chest as follows:

- right upper chest (second intercostal space, midclavicular line)
- right lower chest (fourth intercostal space, midclavicular line)
- right axilla (sixth intercostal space, midaxillary line)
- right upper back (second intercostal space, between medial scapular edge and spine)
- right midback (fifth intercostal space, between medial scapular edge and spine)
- right lower back (eighth intercostal space, just inferior to tip of scapula)
- left upper chest (second intercostal space, midclavicular line)
- left lower chest (fourth intercostal space, midclavicular line)
- left axilla (sixth intercostal space, midaxillary line)
- left upper back (second intercostal space, between medial scapular edge and spine)
- left midback (fifth intercostal space, between medial scapular edge and spine)
- left lower back (eighth intercostal space, just inferior to tip of scapula)
- suprasternal notch.

Following attachment the devices, participants took five deep breaths, inhaling and exhaling fully. Patient information was obtained retrospectively from their medical records, including demographic data, smoking status, medical history, spirometry data, vital signs and results from diagnostic tests, including CT images.

The authors affirm that parents or legal guardians of the children included in the study provided written informed consent for publication of the images in Figs. 3 and 4 and Supplementary Figs. 11 and 13.

Data statistics

Statistical analysis was performed with one-way multivariate analysis of variance in MATLAB, with an assumption that data points for each group are normally distributed. Analysis of neonatal heart rate involved the use of 136,013 body sound data points and FDA-approved ECG monitor data collected from five neonates (nos. B001–B005; Extended Data Table 1). Respiratory data analysis utilized a cumulative 43,750 body sound data points, 43,738 nasal temperature recordings

and 1,012 pneumotach data points collected from 15 neonates (nos. A001–A010 and B001–B005; Extended Data Table 1). Bowel sound analysis was performed on data collected from three neonates (nos. C001–003), consisting of 251 bowel sound peak data (Extended Data Table 1). Lung sound analysis was conducted on 10,660 lung sound datapoints collected from 20 healthy participants and 35 patients with chronic lung disease (nos. D001–D055) using 13 BAMS devices (Extended Data Table 1).

Reporting summary

Further information on research design is available in the Nature Portfolio Reporting Summary linked to this article.

Data availability

The data used in the study are not publicly available because they contain information that could compromise research participant privacy. Anonymized data can be made available on request for academic purposes. Sample data of cardiorespiratory signals from a healthy participant are available at https://github.com/JY9292/BAMS_System.

Code availability

The analysis code that supports the findings of this study is available at https://github.com/JY9292/BAMS_System.

References

44. Mohanarangam, K., Palagani, Y. & Choi, J. R. Evaluation of specific absorption rate in three-layered tissue model at 13.56 MHz and 40.68 MHz for inductively powered biomedical implants. *Appl. Sci.* **9**, 1125 (2019).

Author contributions

J.-Y.Y., S.O., W.S., W.-Y.M., E.C., G.M.S., D.E.W.-M., A. Bharat and J.A.R. conceived the idea, designed the research and wrote the manuscript. J.-Y.Y., S.O., W.-Y.M., M.-K.C., M.P., S.S., S.Y., G.K. and H.J. designed the device and carried out fabrication. J.-Y.Y. designed operation protocols and the graphical user interface. J.-Y.Y., W.S., E.C., E.J., S.L., A.T. and A. Bharat analyzed data. J.-Y.Y., S.O., W.S., E.C., E.J., M.C., S.L., Y.W., E.O., A. Banks, G.M.S., D.E.W.-M., A. Bharat and J.A.R. carried out experimental validation and analysis. All authors have read and approved the manuscript.

Competing interests

The authors declare no competing interests.

Additional information

Extended data is available for this paper at https://doi.org/10.1038/s41591-023-02637-5.

Supplementary information The online version contains supplementary material available at https://doi.org/10.1038/s41591-023-02637-5.

Correspondence and requests for materials should be addressed to Ankit Bharat or John A. Rogers.

Peer review information *Nature Medicine* thanks C. Mascolo, J. Ho, J. DiFiore and S. Niu for their contribution to the peer review of this work. Primary Handling Editor: Michael Basson, in collaboration with the *Nature Medicine* team.

Reprints and permissions information is available at www.nature.com/reprints.
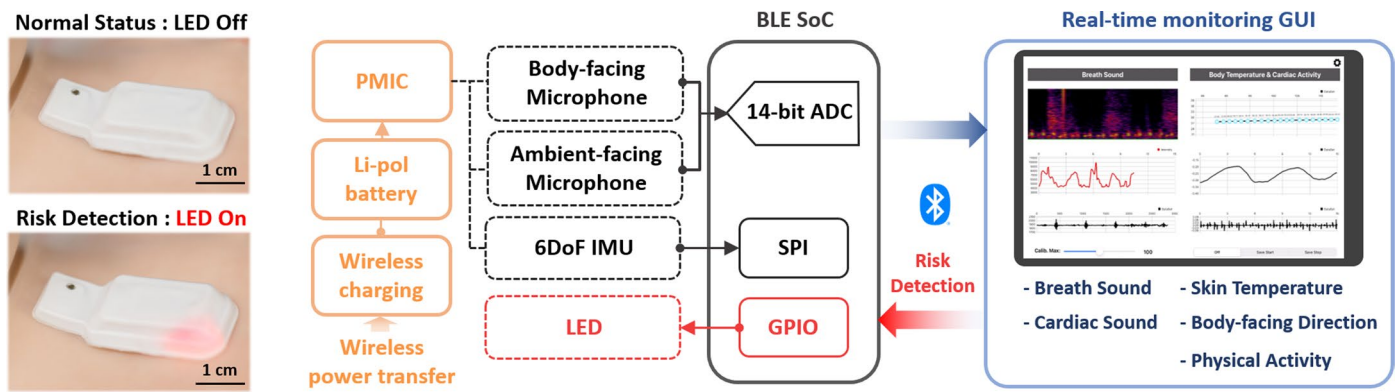
Extended Data Fig. 1 | Design for continuous physiological monitoring system with visual feedback. A photograph of visual feedback and block diagram illustrating the real-time operational scheme.
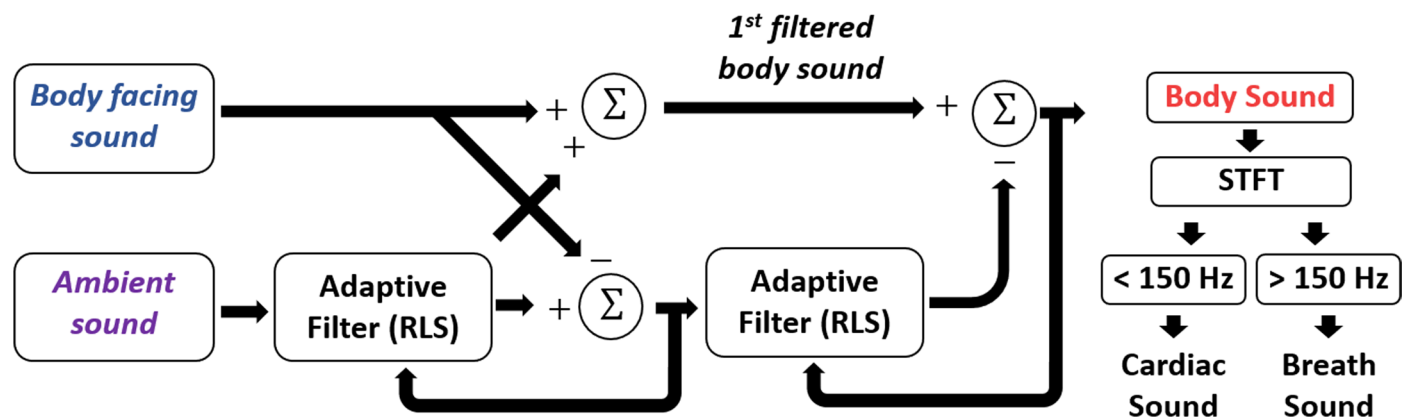
Extended Data Fig. 2 | Flow chart of two-step adaptive acoustic filtering for separate measurements of body and ambient sounds.
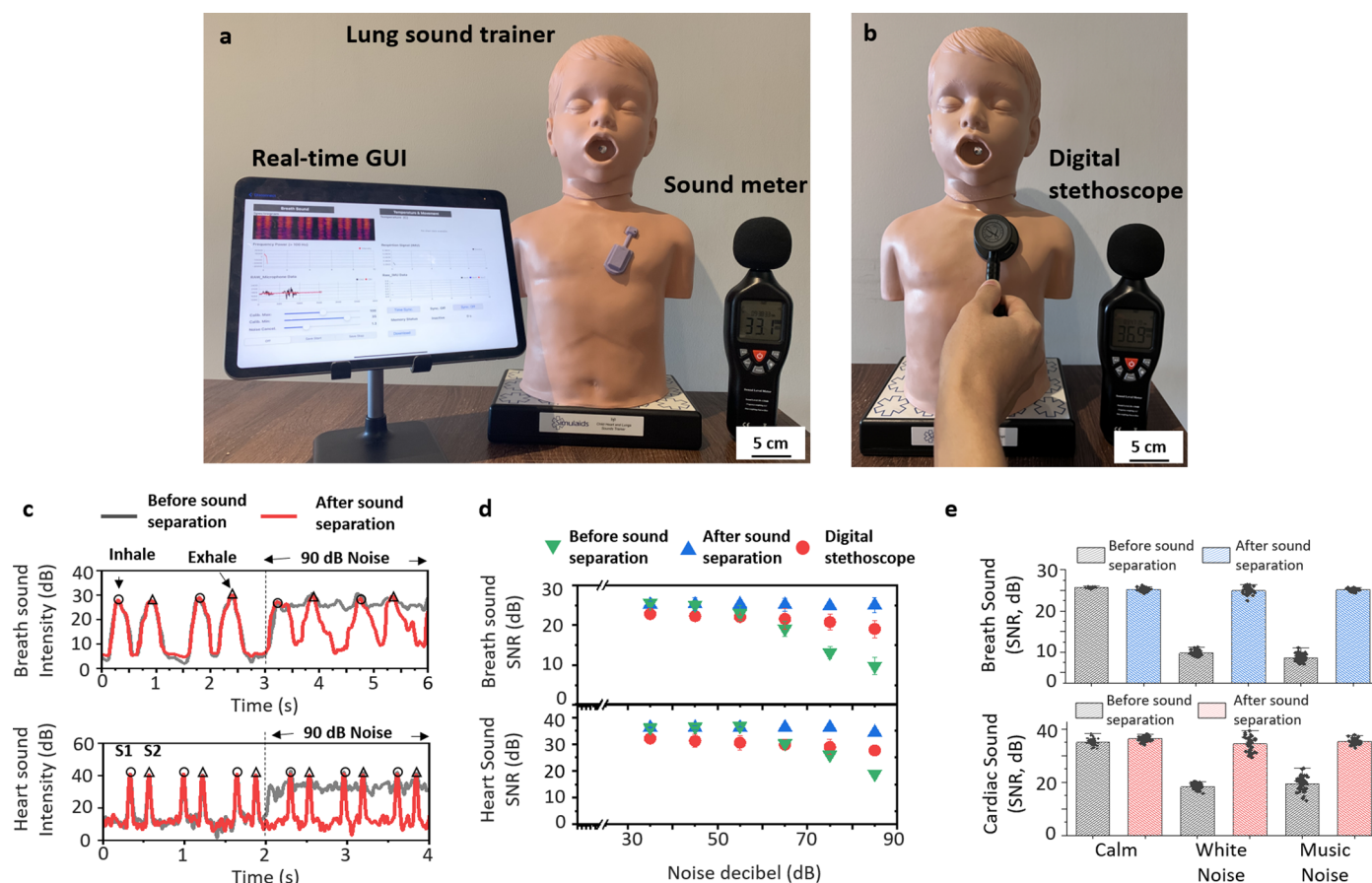
Extended Data Fig. 3 | Characterization of sound separation using the BAMS system. (**a, b**) Experimental setup using a lung sound trainer, sound meter, with (a) a BAMS system and (b) a commercial digital stethoscope (3 M™ Littmann® CORE, Eko) with active noise cancellation (**c**) Breath sound and heart sound intensity recorded in an ambient of 90 dB white noise across frequency from 20 to 400 Hz (**d, e**) Signal-to-noise ratio (SNR) of breath sound and heart sound for the BAMS system and the commercial digital stethoscope, measured in different ambient conditions, including (d) levels of white noise (n = 50 datapoints) and (e) types of sounds with a noise level of 75 dB (n = 50 datapoints). Data are presented as the mean ± standard deviation of SNR.
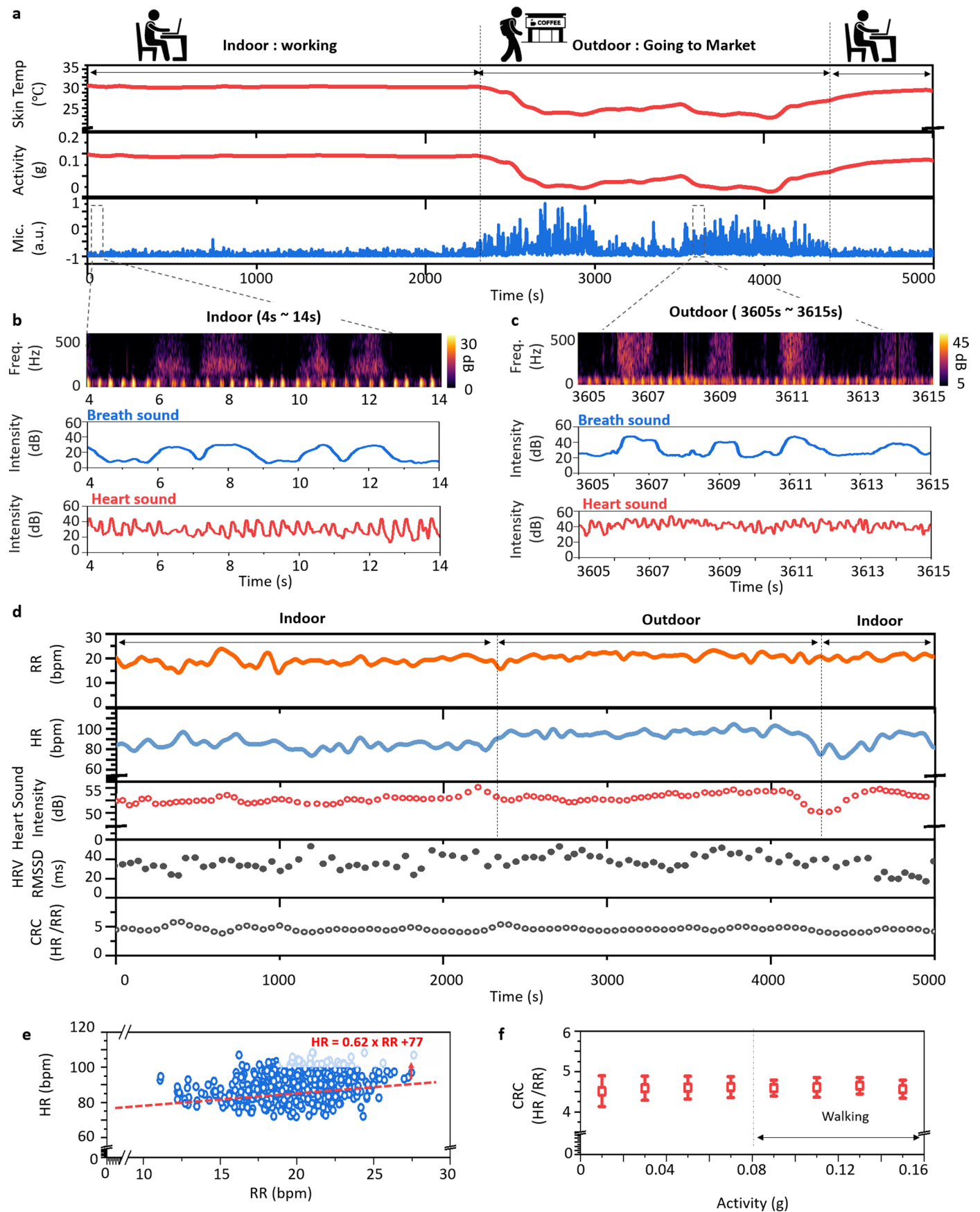
Extended Data Fig. 4 | See next page for caption.

Extended Data Fig. 4 | Cardiopulmonary monitoring and cardio-respiratory coupling analysis during daily activities. (**a**) Data corresponding to skin temperature, physical activity, and body sounds captured during daily activities. (**b, c**) Spectrogram images and intensity of breath and heart sounds as a function of time for recordings collected indoors and outdoors. (**d**) Respiratory rate, heart rate, heart sound intensity, heart rate variability, and cardio-respiratory coupling extracted from data collected indoors and outdoors. (**e**) Correlation between heart rate and respiratory rate (n = 4291 datapoints). (**f**) Cardio-respiratory coupling values as a function of physical activity levels (n = 4291 datapoints). Data are presented as the mean ± standard deviation of cardio-respiratory coupling values.
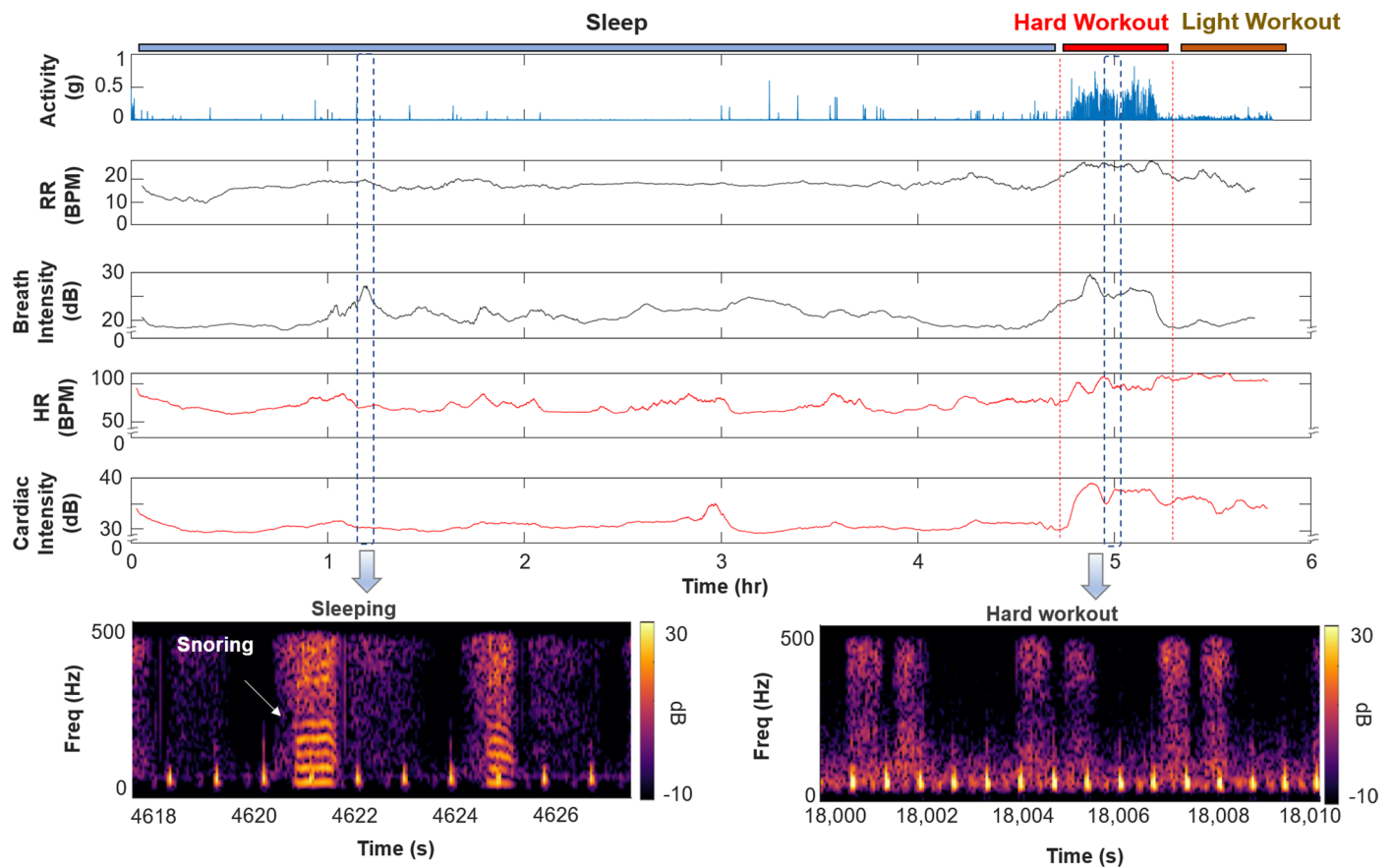
Extended Data Fig. 5 | Continuous long-term cardiorespiratory monitoring during sleep and vigorous activity. Spectrogram image of cardiorespiratory signal and time series results of activity, respiratory rate, breath sound intensity, heart rate, and cardiac sound intensity.
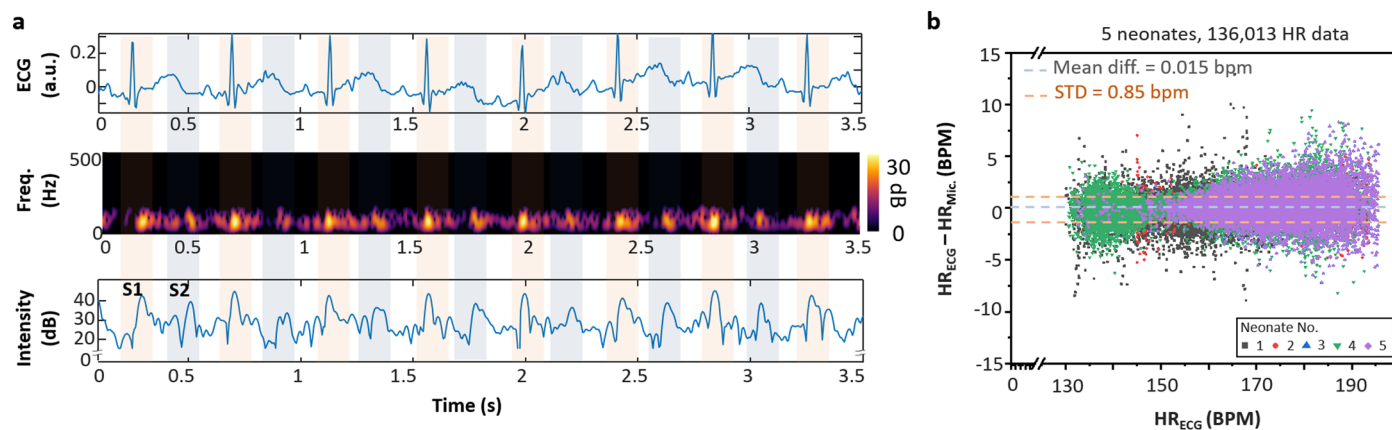
Extended Data Fig. 6 | Monitoring of neonatal cardiac activity using the BAMS system. (**a**) ECG signal, spectrogram image, and heart sound intensity. (**b**) Bland-Altman plots comparing heart rate determined using the BAMS system with ECG measurements (5 neonates, 136,013 data points).
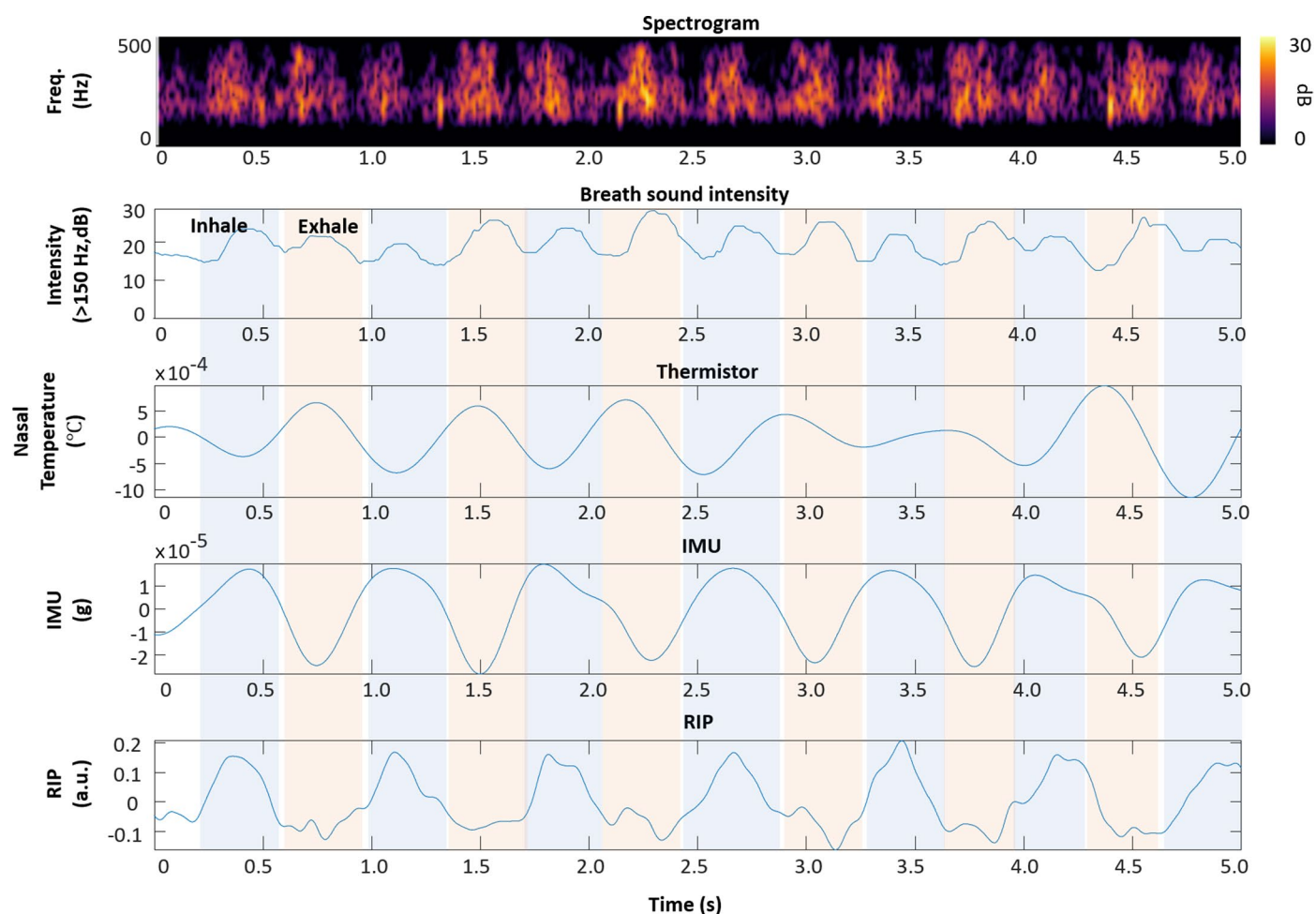
Extended Data Fig. 7 | Monitoring of neonatal respiratory behavior using the BAMS system, nasal thermistor, and respiratory inductance plethysmograms. Spectrogram images and time series results comparing respiratory behaviors obtained from breath sounds measured with the microphone in a BAMS system, temperature measured with a nasal thermistor, chest wall movement measured with the IMU in a BAMS system, and the summation of respiratory inductance plethysmograms measured with chest and abdomen RIP bands.
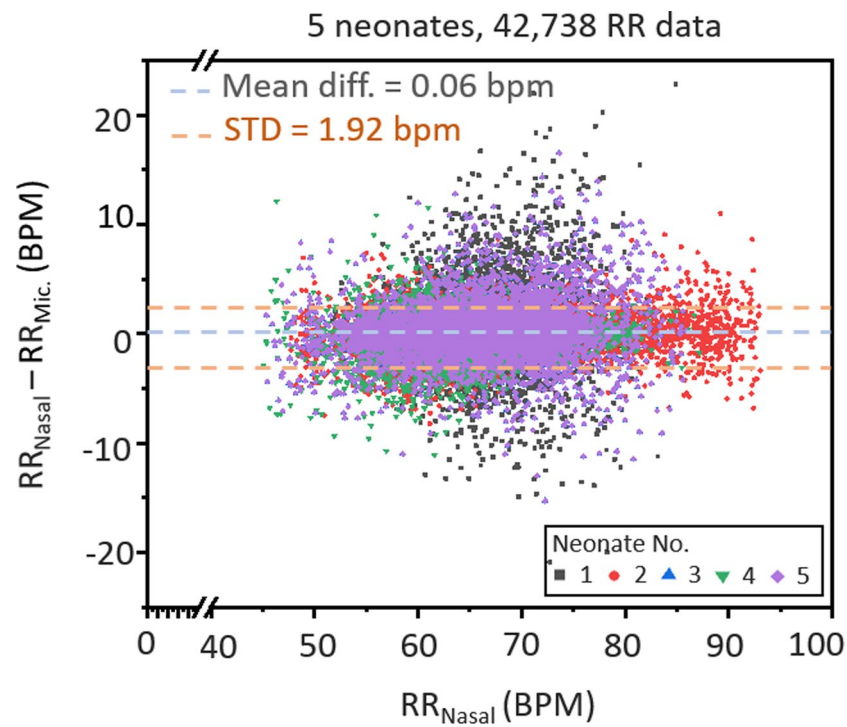
Extended Data Fig. 8 | Respiratory rate data collected in the NICU and comparisons to standard measurements. Bland-Altman plots comparing respiratory rate determined using the BAMS system with nasal temperature flow measurements (5 neonates, 42,738 data points).

a

b

c

d
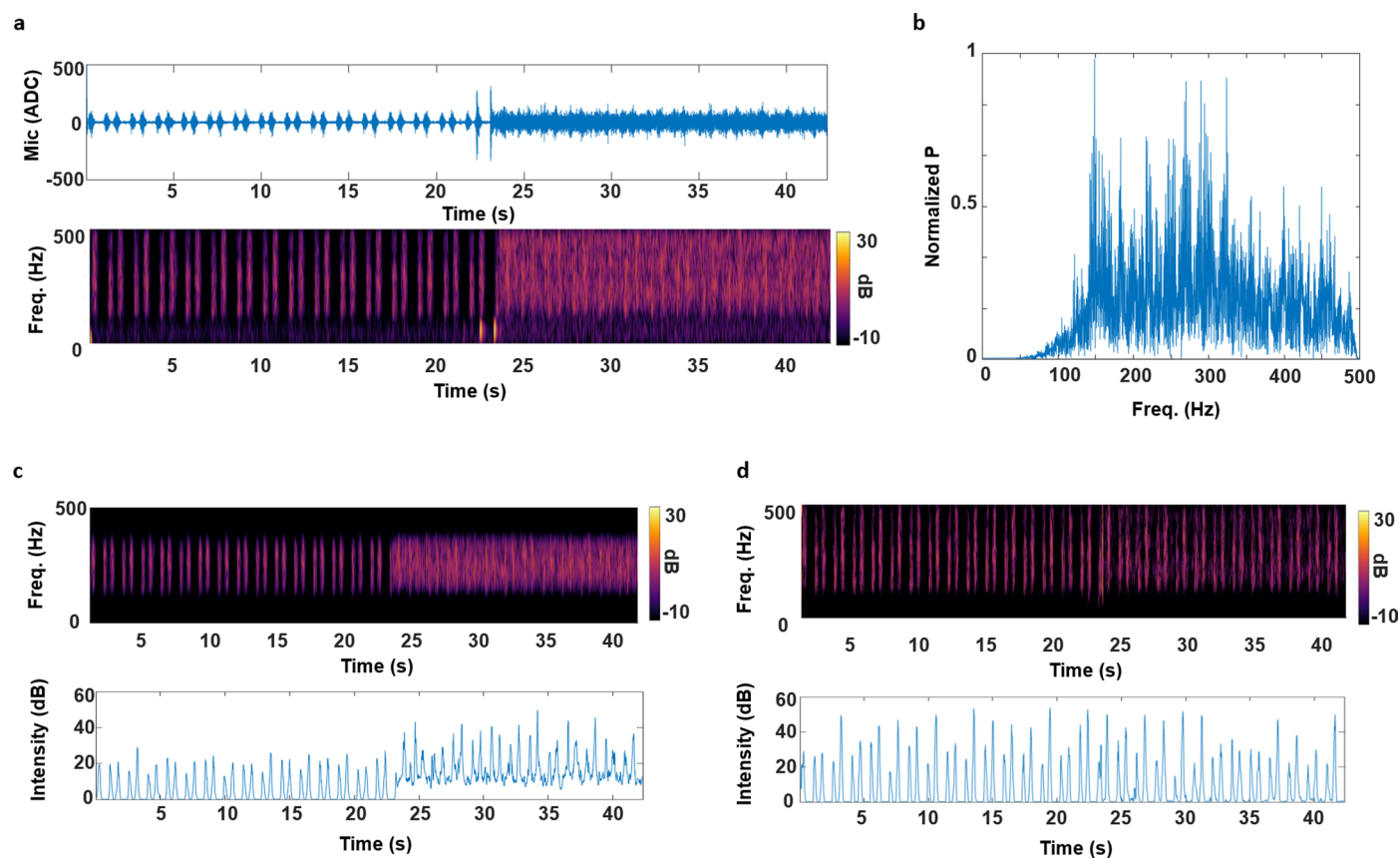
Extended Data Fig. 9 | Effects of ambient noise on measurements of respiratory sounds. (**a**) Microphone data and spectrogram image of respiratory sounds with and without 70 dB white noise. (**b**) Frequency distribution of respiratory sounds determined by FFT of recorded data. (**c**) Spectrogram image and respiratory sound intensity with bandpass filtering from 150 Hz to 300 Hz, and (**d**) spectrogram image and respiratory sound intensity with sound separation.

Extended Data Table 1 | Participant characteristics

Study ID	Gestational age (weeks)	Postmenstrual age (weeks)	Years old	Weight(kg)	BMI (kg/m^2)	Sex
A001	31 weeks	34 weeks		2 kg		Female
A002	30 weeks	33 weeks		2 kg		Female
A003	28 weeks	36 weeks		3 kg		Female
A004	28 weeks	34 weeks		2 kg		Male
A005	30 weeks	34 weeks		2 kg		Female
A006	28 weeks	36 weeks		2 kg		Female
A007	26 weeks	34 weeks		2 kg		Female
A008	25 weeks	36 weeks		3 kg		Male
A009	29 weeks	34 weeks		2 kg		Male
A010	25 weeks	35 weeks		3 kg		Male
B001	26 weeks	35 weeks		2 kg		Female
B002	29 weeks	35 weeks		2 kg		Male
B003	25 weeks	35 weeks		3 kg		Male
B004	30 weeks	33 weeks		2 kg		Female
B005	30 weeks	33 weeks		2 kg		Female
C001	29 weeks	38 weeks		3 kg		Male
C002	28 weeks	35 weeks		2 kg		Female
C003	29 weeks	37 weeks		3 kg		Female
D001			79 years old		31 kg/m^2	Female
D002			76 years old		17 kg/m^2	Female
D003			73 years old		30 kg/m^2	Female
D004			78 years old		25 kg/m^2	Female
D005			84 years old		26 kg/m^2	Female
D006			68 years old		24 kg/m^2	Female
D007			66 years old		31 kg/m^2	Male
D008			70 years old		26 kg/m^2	Male
D009			60 years old		20 kg/m^2	Female
D010			74 years old		24 kg/m^2	Female
D011			58 years old		20 kg/m^2	Male
D012			75 years old		28 kg/m^2	Male
D013			71 years old		23 kg/m^2	Female
D014			70 years old		24 kg/m^2	Female
D015			79 years old		24 kg/m^2	Female
D016			59 years old		21 kg/m^2	Male
D017			63 years old		28 kg/m^2	Female
D018			69 years old		29 kg/m^2	Female
D019			77 years old		36 kg/m^2	Female
D020			56 years old		41 kg/m^2	Male
D021			74 years old		30 kg/m^2	Male
D022			52 years old		34 kg/m^2	Male
D023			19 years old		30 kg/m^2	Male
D024			52 years old		25 kg/m^2	Female
D025			76 years old		30 kg/m^2	Female
D026			70 years old		41 kg/m^2	Female
D027			63 years old		18 kg/m^2	Female
D028			51 years old		27 kg/m^2	Male
D029			56 years old		31 kg/m^2	Male
D030			69 years old		24 kg/m^2	Male
D031			68 years old		22 kg/m^2	Male
D032			67 years old		26 kg/m^2	Male
D033			62 years old		29 kg/m^2	Female
D034			45 years old		30 kg/m^2	Male
D035			73 years old		27 kg/m^2	Female
D036			69 years old		28 kg/m^2	Female
D037			72 years old		27 kg/m^2	Male
D038			34 years old		39 kg/m^2	Male
D039			49 years old		21 kg/m^2	Female
D040			24 years old		27 kg/m^2	Male
D041			33 years old		28 kg/m^2	Male
D042			31 years old		26 kg/m^2	Male
D043			31 years old		34 kg/m^2	Male
D044			25 years old		34 kg/m^2	Male
D045			19 years old		29 kg/m^2	Male
D046			36 years old		27 kg/m^2	Male
D047			45 years old		31 kg/m^2	Male
D048			31 years old		29 kg/m^2	Male
D049			35 years old		21 kg/m^2	Male
D050			37 years old		37 kg/m^2	Male
D051			41 years old		29 kg/m^2	Male
D052			30 years old		34 kg/m^2	Male
D053			24 years old		21 kg/m^2	Male
D054			26 years old		25 kg/m^2	Male
D055			43 years old		33 kg/m^2	Male

Participants A001-A010 underwent 10-minute respiratory monitoring in the NICU; participants B001-B005 underwent 3-hour respiratory monitoring in the NICU; participants C001-C003 underwent bowel sound monitoring in the NICU; participants D001-D055 underwent lung sound monitoring in thoracic surgery clinic (D001-D035 were patients with chronic lung disease, D036-D055 were healthy participants).

nature portfolio

Corresponding author(s): John A. Rogers

Last updated by author(s): Oct 6, 2023

Reporting Summary

Nature Portfolio wishes to improve the reproducibility of the work that we publish. This form provides structure for consistency and transparency in reporting. For further information on Nature Portfolio policies, see our Editorial Policies and the Editorial Policy Checklist.

Statistics

For all statistical analyses, confirm that the following items are present in the figure legend, table legend, main text, or Methods section.

n/a	Confirmed	
☐	☒	The exact sample size (*n*) for each experimental group/condition, given as a discrete number and unit of measurement
☐	☒	A statement on whether measurements were taken from distinct samples or whether the same sample was measured repeatedly
☐	☒	The statistical test(s) used AND whether they are one- or two-sided *Only common tests should be described solely by name; describe more complex techniques in the Methods section.*
☐	☒	A description of all covariates tested
☐	☒	A description of any assumptions or corrections, such as tests of normality and adjustment for multiple comparisons
☐	☒	A full description of the statistical parameters including central tendency (e.g. means) or other basic estimates (e.g. regression coefficient) AND variation (e.g. standard deviation) or associated estimates of uncertainty (e.g. confidence intervals)
☐	☒	For null hypothesis testing, the test statistic (e.g. *F*, *t*, *r*) with confidence intervals, effect sizes, degrees of freedom and *P* value noted *Give P values as exact values whenever suitable.*
☒	☐	For Bayesian analysis, information on the choice of priors and Markov chain Monte Carlo settings
☒	☐	For hierarchical and complex designs, identification of the appropriate level for tests and full reporting of outcomes
☐	☒	Estimates of effect sizes (e.g. Cohen's *d*, Pearson's *r*), indicating how they were calculated

Our web collection on statistics for biologists contains articles on many of the points above.

Software and code

Policy information about availability of computer code

Data collection	Data was collected from a customized Bluetooth protocol-based App developed using Xcode (V15.0).
Data analysis	Data analysis was performed using MATLAB (MathWork, Version R2023b).

For manuscripts utilizing custom algorithms or software that are central to the research but not yet described in published literature, software must be made available to editors and reviewers. We strongly encourage code deposition in a community repository (e.g. GitHub). See the Nature Portfolio guidelines for submitting code & software for further information.

Data

Policy information about availability of data

All manuscripts must include a data availability statement. This statement should provide the following information, where applicable:
- Accession codes, unique identifiers, or web links for publicly available datasets
- A description of any restrictions on data availability
- For clinical datasets or third party data, please ensure that the statement adheres to our policy

The data used in the study are not publicly available because they contain information that could compromise research participant privacy. Anonymized data can be made available upon request for academic purposes. Sample data of cardiorespiratory signals of a healthy participant are available at https://github.com/JY9292/BAMS_System.

Research involving human participants, their data, or biological material

Policy information about studies with <u>human participants or human data</u>. See also policy information about <u>sex, gender (identity/presentation), and sexual orientation</u> and <u>race, ethnicity and racism</u>.

Reporting on sex and gender	We included a total of 15 neonates and 55 adults in our study, without consideration of their sex or gender. The selection of participants was based solely on their suitability for the research objectives.
Reporting on race, ethnicity, or other socially relevant groupings	Race or ethnicity is not a relevant factor in our study.
Population characteristics	A total of 15 neonates, with a post-menstrual age ranging from 33 to 36 weeks, and 55 adults, ranging in age from 18 to 84 years, participated in this study. We presented the detailed information in Expended Data Table 1.
Recruitment	All recruitment took place at Northwestern Medicine and McGill University Health Center. A member of the McGill University Health Center research team approached each family that had expressed interest in participating to assess their suitability. Following a doctor consultation, a member of the Northwestern Medicine research team approached patients who had expressed interest in participating to assess their suitability. We recruited both healthy participants and patients with chronic lung disease. We believe our analysis was not impacted as a wider cohort will only strengthen the results.
Ethics oversight	The study protocol was approved by the Northwestern Medicine Institutional Review Board (STU00218021) and the McGill University Health Center Research Ethics Board (IRB00010120).

Note that full information on the approval of the study protocol must also be provided in the manuscript.

Field-specific reporting

Please select the one below that is the best fit for your research. If you are not sure, read the appropriate sections before making your selection.

☒ Life sciences ☐ Behavioural & social sciences ☐ Ecological, evolutionary & environmental sciences

For a reference copy of the document with all sections, see <u>nature.com/documents/nr-reporting-summary-flat.pdf</u>

Life sciences study design

All studies must disclose on these points even when the disclosure is negative.

Sample size	Data of 70 participants have been used in this study. The analysis of neonatal heart rate involved the use of 136,013 body sound datapoints and FDA-approved ECG monitor data collected from 5 neonates. Respiratory data analysis utilized a cumulative 43,750 body sound datapoints, 43,738 nasal temperature recordings, and 1,012 pneumotach datapoints collected from 15 neonates. Bowel sound analysis was performed on data collected from 3 neonates, consisting of 251 bowel sound peaks data. Lung sound analysis was conducted on 10,660 lung sound datapoints collected from 20 healthy participants and 35 patients with chronic lung disease, using 13 BAMS devices.
Data exclusions	No data was excluded.
Replication	Results were replicated in independent experiments as described in the manuscript. Every experiment included replicates as described in the method section.
Randomization	This is not relevant to this study. We conducted a prospective, observational single-arm study to evaluate the safety and performance of our sensors. Thus, randomization was not necessary or appropriate.
Blinding	We conducted a prospective, observational clinical study to evaluate the safety and performance of our sensors. Nurses / patients /clinicians were not blinded to use of the sensors.

Reporting for specific materials, systems and methods

We require information from authors about some types of materials, experimental systems and methods used in many studies. Here, indicate whether each material, system or method listed is relevant to your study. If you are not sure if a list item applies to your research, read the appropriate section before selecting a response.

Materials & experimental systems

n/a	Involved in the study
☒ ☐	Antibodies
☒ ☐	Eukaryotic cell lines
☒ ☐	Palaeontology and archaeology
☒ ☐	Animals and other organisms
☒ ☐	Clinical data
☒ ☐	Dual use research of concern
☒ ☐	Plants

Methods

n/a	Involved in the study
☒ ☐	ChIP-seq
☒ ☐	Flow cytometry
☒ ☐	MRI-based neuroimaging